Numerical Analysis for Partial Differential Equations

H(div)-conforming Finite Element Methods for the Darcy's Problem

Prof. Simona Perotto

A. Y. 2014-2015

Domenico Notaro 80443

domenico.notaro@mail.polimi.it

Contents

Abstract

We consider the problem of Darcy flow which is notoriously of considerable practical importance in civil, geotechnical, and petroleum engineering [18]. Moreover, recent works in the field of biomedical engineering (see, e.g., [14]) show that the Darcy law is a valid assumption while modeling the tissue perfusion in biological tissues.

Currently, numerical methods are based on two different approaches: one involves a *primal*, single-field formulation for pressure; and the other employs a *mixed* two-field formulation in which pressure and velocity are variables. The primal formulation amounts to solving a Poisson problem for pressure with a rough coefficient (i.e., the ratio of permeability to viscosity). This can be done with adequate accuracy using existing finite element methodology. However, it is the derived flux, that is, the velocity, which is of primary interest. In this formulation it is obtained by taking the gradient of pressure and multiplying it by the rough coefficient. There is typically a loss of accuracy in the process and, additionally, mass conservation is not guaranteed. Consequently, this basic approach has not proved adequate for practical engineering applications. An improved variant on this theme, which involves a post-processing of the velocity field to improve accuracy and enforce mass conservation, has proved to be a viable option (see, e.g., [16] and references therein). The more popular approach in applications so far has been based on the mixed formulation (e.g., [2]). The classical mixed variational formulation is posed in terms of the function spaces $L^2(\Omega)$ and $\mathbf{H}(\mathrm{div}, \Omega)$ for the pressure and velocity, respectively. It has been a challenge to develop finite element approximations of these spaces, which satisfy the celebrated Babuska–Brezzi, or inf–sup, stability condition [1, 6]. These discrete spaces have been used successfully in numerous applications. Good accuracy has been attained for both velocity and pressure, and mass conservation is achieved locally (i.e., element-wise) as well as globally. However, this approach also has its drawback: complexity. Different interpolations are required for pressure and velocity (and concentration in simulation of miscible displacements in porous media) and implementation is particularly complicated in three dimensions. Velocities are required to have continuous normal components across element interfaces, whereas tangential components are discontinuous. Pressure fields are discontinuous and must not be of too high order, otherwise the inf–sup condition is violated. Only normal velocity degrees of freedom are present on element interfaces while all velocity degrees of freedom are present in element interiors. Within the classical mixed variational framework, this is the price one pays for success.

The work is organized as follows. In Section 1 we briefly discuss the main theoretical aspects of the Mixed Finite Element Method (MFEM). This part is strongly inspired by the standard reference on mixed methods: Brezzi and Fortin [10]. The mathematical formulation of the Darcy problem is addressed in Section 2. We derive two variational formulations: the standard pressure formulation in $H^1(\Omega)$ and a mixed pressure-velocity formulation in $\left(L^2(\Omega), \mathbf{H}(\mathrm{div}, \Omega)\right)$. The section ends with the analysis of well-posedness of the mixed problem, belonging to the context of the *Theory of Saddle-Point Problems* [10]. The discretization of the above weak formulation is achieved in Section 3 by means of the Galerkin-FEM. Specifically, we propose two families of methods for the primal problem (Lagrange, non-conforming Crouzeix-Raviart) and three families of H(div)-conforming mixed methods (Raviart-Thomas, Brezzi-Douglas-Marini, Brezzi-Douglas-Fortin-Marini). At the end of the section we provide a quantitative comparison

of the above FEM in terms of approximation accuracy. The objective of Section 4 is, ideed, to verify such theoretical predictions by implementing a benchmark problem in *FreeFem++* [15]. We perform fairly extensive convergence tests which confirm the theoretical error estimate for all elements considered. Finally, in Appendix A we give further details about the implementation.

1 Mixed Finite Element Methods for Problems in H(div)

In light of future applications to the Darcy law on a given domain Ω, we introduce some finite dimensional subspaces of $\mathbf{H}(\mathrm{div}, \Omega)$ and $L^2(\Omega)$ made of piecewise polynomial functions.

For simplicity we will consider the case of simplicial elements - i.e. triangles in 2D and four-point tetrahedra in 3D (for generalizations to higher dimensions see [5]) - and the associated Raviart-Thomas spaces which are the best-known spaces for this problem. This family of spaces was introduced in [23] in the two dimensional case, while its extension to three dimensions was first considered in [19]. Since no essential technical difficulties arise in the general case, we prefer to present the spaces and the analysis of their properties in the general n-dimensional case (although, of course, we are mainly interested in the cases $n = 2$ and $n = 3$). Below we will comment and give references on different variants of spaces.

First we introduce the local spaces, analyze their properties and construct the Raviart-Thomas interpolation.

1.1 Simplicial approximation of H(div)

Let us introduce some notations. We shall denote by $\{\mathcal{T}_h\}$ a family of simplicial mesh, i.e. of partitions of Ω into elements (i.e. $\Omega = \bigcup_{K\in\mathcal{T}_h} K$). The apex h is a measure of the mesh-size, namely, $h = max_{K\in\mathcal{T}_h} h_K$, being $h_K = \mathrm{diam}(K)$. In practical cases, K will be a triangle or a quadrilateral (resp., a tetrahedron or a hexahedron in three dimensions) and we shall call it element. For simplicity we restrict the analysis to the case of simplicial elements. The edges of each element K will be denoted by e_i with $i = 1, 2, 3$ in the two-dimensional case. For three-dimensional elements, unless differently stated, we denote again the faces of the elements by e_i with $i = 1, 2, 3, 4$. Note that for a fixed dimension n, the edges are $(n-1)$-dimensional simplices. We denote with $\mathcal{E}_h$ the set of all edges in $\mathcal{T}_h$, namely $\mathcal{E}_h = \bigcup_{K\in\mathcal{T}_h} \partial K$. The corresponding unit outward normals are referred to as $\mathbf{n}_i$. We also denote by

$$e_{ij} = \partial K_i \cap \partial K_j$$

the interface between element K_i and K_j. We only deal with *compatible* meshes in the sense that the intersection between two elements is a common face, side or vertex. The situation when a mesh contains hanging nodes is out of the aims of this work. As a consequence, we have that $\mathcal{E}_h$ coincides with the union of all interfaces and all boundary edges (or faces). Moreover, we assume that the family of triangulations is regular, i.e., for any $K \in \mathcal{T}_h$ and

any h, the following regularity condition is satisfied with a uniform σ:

$$\frac{h_K}{\rho_K} \;\leq\; \sigma \tag{1}$$

with ρ_K diameter of the largest ball inscribed in K.

As for classical Sobolev space $H^m(\Omega)$, we want to build approximation of $\mathbf{H}(\mathrm{div},\Omega)$ that are locally polynomial.We indicate with $\mathcal{P}_k$ the standard space of polynomials of degree $\leq k$ in the variables $\mathbf{x} = (x_1, \ldots, x_n)$. We shall also need polynomial spaces on the edges (or faces) of the elements, namely

$$\mathcal{R}_k(\partial K) := \left\{\; \phi \in L^2(\partial K) \;:\; \phi\,|_{e_i} \in \mathcal{P}_k(e_i) \quad \forall\, e_i \;\right\}. \tag{2}$$

Functions of $\mathcal{R}_k(\partial K)$ are polynomials of degree $\leq k$ on each side (or face) of K. They do not have to be continuous at vertices. Moreover, we will need in the next section the following definition, originally given by Nédélec [19] for the approximation of $\mathbf{H}(\mathrm{curl},\Omega)$

$$\boldsymbol{\mathcal{N}}_k(K) := \mathcal{P}_k(K;\mathbb{R}^n) \oplus [\,\mathbf{x} \wedge \mathcal{P}_k^h(K;\mathbb{R}^n)\,], \tag{3}$$

where $\mathcal{P}_k^h$ denotes the space of homogeneous polynomials of degree k. Following [10] we define for arbitrary indexes $k \geq 0$, $s \leq k$

$$\mathcal{P}_k^s(K;\mathbb{R}^n) := \left\{\; \mathbf{w} \in \mathcal{P}_k(K;\mathbb{R}^n) \;:\; \mathbf{w}\cdot\mathbf{n} \in \mathcal{R}_s(\partial K) \;\right\} \tag{4}$$

and

$$\mathcal{P}_{\mathbf{k}+\mathbf{x}\,k}^s(K;\mathbb{R}^n) := \left\{\; \mathbf{w} \in \mathcal{P}_k(K;\mathbb{R}^n) + \mathbf{x}\,\mathcal{P}_k(K) \;:\; \mathbf{w}\cdot\mathbf{n} \in \mathcal{R}_s(\partial K) \;\right\}. \tag{5}$$

As we will see in the remainder, the above definitions allow us to derive a unified classification of all the families of $\mathbf{H}(\mathrm{div},\Omega)$-conforming spaces we will use. The case $s = k$ is the most natural and widely used. Taking $s \leq k-1$ defines what we shall call *reduced* spaces. We introduce special names for a few classical cases. For $s = k$, the space $\mathcal{P}_k^k$ was introduced in [9] (for $n = 2$) and [7] (for $n = 3$). We shall thus call it the local *Brezzi-Douglas-Marini* (BDM) space of order $k \geq 1$ and write,

$$\mathcal{BDM}_k(K) := \mathcal{P}_k^k(K;\mathbb{R}^n) \;. \tag{6}$$

The space $\mathcal{P}_{\mathbf{k}+\mathbf{x}\,k}^k$ was defined in [19] following [23]. We shall call it the local *Raviart-Thomas* (RT) space of order $k \geq 0$ and write

$$\mathcal{RT}_k(K) := \mathcal{P}_{\mathbf{k}+\mathbf{x}\,k}^k(K;\mathbb{R}^n) \;. \tag{7}$$

Finally the reduced case $\mathcal{P}_k^{k-1}$ was considered in [8] and we call it the local *Brezzi-Douglas-Fortin-Marini* (BDFM) space of order $k \geq 1$ and write

$$\mathcal{BDFM}_k(K) := \mathcal{P}_k^{k-1}(K;\mathbb{R}^n) \;. \tag{8}$$

For the simplicial case, we thus have the following inclusions between the spaces just defined:

$$\mathcal{RT}_{k-1} \subset \mathcal{BDFM}_k \subset \mathcal{BDM}_k \subset \mathcal{RT}_k \subset \mathcal{BDFM}_{k+1} \subset \mathcal{BDM}_{k+1} \subset \dots \ . \tag{9}$$

We now have to define suitable degrees of freedom such that continuity of $\mathbf{w} \cdot \mathbf{n}$ at the interfaces holds. This will allow us to build from $\mathcal{P}_k^s$ an approximation of $\mathbf{H}(\mathrm{div}, \Omega)$. We refer again to [10] for a constructive derivation of these set of values. It is an highly technical argument in which different intermediate results of orthogonality and dimensionality play together to identify the proper degrees of freedom for each of the three families. In Figure 1 we only give a schematic representation of the degrees of freedom of first-order elements $\mathcal{RT}_0$, $\mathcal{BDM}_1$, $\mathcal{RT}_1$ in $\mathbb{R}^2$, second-order elements $\mathcal{BDM}_2$, $\mathcal{BDFM}_2$ in $\mathbb{R}^2$ and the simplest elements $\mathcal{RT}_0$, $\mathcal{BDM}_1$, $\mathcal{RT}_1$ in $\mathbb{R}^3$. Concerning for example the two-dimensional case, it can be seen that the local lowest-order Raviart-Thomas space $\mathcal{RT}_0$ has dimension 3 and we can specify it by the three normal component of the unknown $\mathbf{w}$ on ∂K. Moreover we note that $\mathrm{div}(\mathcal{BDM}_1) = \mathrm{div}(\mathcal{RT}_0) = \mathcal{P}_0$. In the same way, $\mathcal{BDM}_1$ is the subset of $\mathcal{RT}_1$ such that $\mathrm{div}\,\mathbf{w} \in \mathcal{P}_0$ instead of $\mathcal{P}_1$. The same concepts can be extended to $\mathcal{BDM}_2$ and $\mathcal{BDFM}_2$.

1.2 Global approximation of H(div)

Finally, we can define *global* approximation spaces for $\mathbf{H}(\mathrm{div}, \Omega)$ starting from the local spaces (6),(7),(8). Thanks to the choice of degrees of freedom we are automatically guarantee that continuity of normal derivatives at interfaces of elements is satisfied. Given a family $\{\mathcal{T}_h\}$ of triangulations Ω, we define for $k \geq 1$

$$\mathcal{BDM}_k(\Omega, \mathcal{T}_h) := \left\{ \ \mathbf{w} \in \mathbf{H}(\mathrm{div}, \Omega) \ : \ \mathbf{w}|_K \in \mathcal{BDM}_k(K) \quad \forall\ K \in \mathcal{T}_h \ \right\} \tag{10}$$

$$\mathcal{RT}_{k-1}(\Omega, \mathcal{T}_h) := \left\{ \ \mathbf{w} \in \mathbf{H}(\mathrm{div}, \Omega) \ : \ \mathbf{w}|_K \in \mathcal{RT}_{k-1}(K) \quad \forall\ K \in \mathcal{T}_h \ \right\} \tag{11}$$

$$\mathcal{BDFM}_k(\Omega, \mathcal{T}_h) := \left\{ \ \mathbf{w} \in \mathbf{H}(\mathrm{div}, \Omega) \ : \ \mathbf{w}|_K \in \mathcal{BDFM}_k(K) \quad \forall\ K \in \mathcal{T}_h \ \right\} \tag{12}$$

When there will be no ambiguity as to the choice of $\mathcal{T}_h$ we will drop it from the definition and call those spaces the global spaces. Moreover, as we mentioned before, it is useful to give a unified definition of local and global approximation spaces. In particular, whenever it may be convenient, we will denote by the symbol $\mathcal{M}_k(K)$ anyone of the above approximations of $\mathbf{H}(\mathrm{div}, K)$. We refer to anyone of the above spaces such that $\mathcal{P}_k(K) \subseteq \mathcal{M}_k(K)$ but $\mathcal{P}_{k+1}(K) \nsubseteq \mathcal{M}_k(K)$. Hence, in the following, $\mathcal{M}_k(K)$ might be, for example, one the following spaces: $\mathcal{BDM}_k(K)$, $\mathcal{RT}_k(K)$, $\mathcal{BDFM}_{k+1}(K)$. Similarly, for each choice of $\mathcal{M}_k(K)$, we define the global space

$$\boldsymbol{\mathcal{M}}_k(\Omega) := \left\{ \ \mathbf{w} \in \mathbf{H}(\mathrm{div}, \Omega) \ : \ \mathbf{w}|_K \in \mathcal{M}_k(K) \ \right\}. \tag{13}$$

1.3 Interpolation Operator and Error Estimates

A fundamental tool in the error analysis is the interpolation operator. As for the construction of approximation spaces, we introduce such operator starting from the single simplex K and

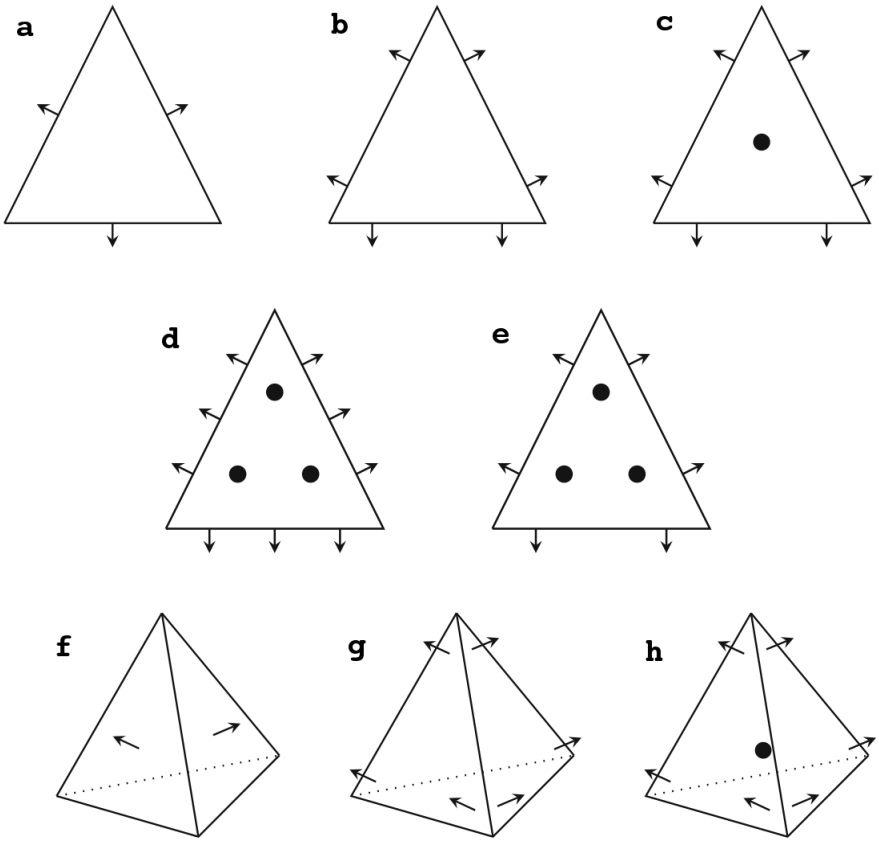

Figure 1: Degrees of freedom of different simplicial approximation of $\mathbf{H}(\mathrm{div}, \Omega)$. Black dots indicate the value of the vectorial unknown $\mathbf{w}$ in K, arrows $\rightarrow$ indicate the value of the normal component $\mathbf{w} \cdot \mathbf{n}$ on ∂K. From top-left to bottom-right we have two-dimensional elements (a) $\mathcal{RT}_0$, (b) $\mathcal{BDM}_1$, (c) $\mathcal{RT}_1$, (d) $\mathcal{BDM}_2$, (e) $\mathcal{BDFM}_2$ and three-dimensional elements (f) $\mathcal{RT}_0$, (g) $\mathcal{BDM}_1$, (h) $\mathcal{RT}_1$

then we use the local definition to build the interpolator over the whole domain Ω. Let now $\mathbf{w} \in \mathbf{H}(\mathrm{div}, K)$ be a given function. Using for each of the spaces the degrees of freedom previously described, it is possible to define an interpolation over the finite-dimensional space, namely $\rho_K \mathbf{w} \in \boldsymbol{\mathcal{M}}_k(K)$. Since the degrees of freedom used always involve the moments of $\mathbf{w}$ on the faces (or sides) of an element, such a construction is possible provided $\mathbf{w}$ is slightly smoother than merely belonging to $\mathbf{H}(\mathrm{div}, \Omega)$. Specifically, it is sufficient[1] to require that the function belongs to the space

$$\boldsymbol{\mathcal{W}}(K) := \left\{ \mathbf{w} \in L^s(K; \mathbb{R}^n) \ : \ \mathrm{div}\, \mathbf{w} \in L^2(\Omega) \right\}, \tag{14}$$

for a fixed $s > 2$. Since the definition of the interpolation operator from $\boldsymbol{\mathcal{W}}(K)$ changes for different choices of the codomain $\boldsymbol{\mathcal{M}}_k(K)$, we shall define it only for the two spaces that interest much in view of future applications.

Definition 1.1 (*Interpolation operator from* $\boldsymbol{\mathcal{W}}(K)$ *to* $\mathcal{P}_k^s(K; \mathbb{R}^n)$)**.** The operator $\rho_K : \boldsymbol{\mathcal{W}}(K) \longrightarrow \mathcal{P}_k^s(K; \mathbb{R}^n)$ is defined by

$$\begin{cases} \displaystyle\int_{\partial K} (\mathbf{w} - \rho_K \mathbf{w}) \cdot \mathbf{n}\, \phi_k \, d\sigma = 0 & \forall\, \phi_k \in \mathcal{R}_k(\partial K) \\ \displaystyle\int_K (\mathbf{w} - \rho_K \mathbf{w}) \cdot \boldsymbol{\psi}_{k-2} \, d\mathbf{x} = 0 & \forall\, \boldsymbol{\psi}_{k-2} \in \boldsymbol{\mathcal{N}}_{k-2}(K) \end{cases} \tag{15}$$

where $\boldsymbol{\mathcal{N}}_k$ has been defined in (3).

Definition 1.2 (*Interpolation operator from* $\boldsymbol{\mathcal{W}}(K)$ *to* $\mathcal{RT}_k(K)$)**.** The operator $\rho_K : \boldsymbol{\mathcal{W}}(K) \longrightarrow \mathcal{RT}_k(K)$ is defined by

$$\begin{cases} \displaystyle\int_{\partial K} (\mathbf{w} - \rho_K \mathbf{w}) \cdot \mathbf{n}\, \phi_k \, d\sigma = 0 & \forall\, \phi_k \in \mathcal{R}_k(\partial K) \\ \displaystyle\int_K (\mathbf{w} - \rho_K \mathbf{w}) \cdot \boldsymbol{\psi}_{k-1} \, d\mathbf{x} = 0 & \forall\, \boldsymbol{\psi}_{k-1} \in \mathcal{P}_{k-1}(K; \mathbb{R}^n) \end{cases} \tag{16}$$

In the remainder we derive an estimate for the local interpolation error of a generic approximation space, no matter how the corresponding interpolation operator is defined. As starting point, we state the following result for functions of $H^m(K; \mathbb{R}^n)$:

Proposition 1.1. Let K be an affine element and ρ_K be the interpolation operator from $\boldsymbol{\mathcal{W}}(K)$ to $\boldsymbol{\mathcal{M}}_k(K)$. There exists a constant $c = c(k, K)$ such that for any $\mathbf{w} \in H^m(K; \mathbb{R}^n)$ we have

$$\| \mathbf{w} - \rho_K \mathbf{w} \|_{s,K} \leq c\, {h_K}^{m-s} |\, \mathbf{w} \,|_{m,K} \qquad 1 \leq m \leq k+1\,,\ s = 0, 1 \tag{17}$$

$\Diamond$

[1] For further details see [10].

In order to analyse the behaviour of the error in $\mathbf{H}(\mathrm{div}, \Omega)$ we need to characterize the space of the divergences of the vectors in $\boldsymbol{\mathcal{M}}_k(K)$, namely

$$\mathcal{D}_k(K) := \mathrm{div}\left(\boldsymbol{\mathcal{M}}_k(K)\right) \ . \tag{18}$$

For an affine simplicial element K, we have

$$\mathrm{div}(\,\mathcal{BDM}_k(K)\,) \;=\; \mathcal{P}_{k-1}(K) \tag{19}$$

$$\mathrm{div}(\,\mathcal{RT}_k(K)\,) \;=\; \mathcal{P}_k(K) \tag{20}$$

$$\mathrm{div}\left(\mathcal{BDFM}_{k+1}(K)\right) \;=\; \mathcal{P}_k(K) \tag{21}$$

Let moreover π_K be the L^2-projection on $\mathcal{D}_k(K)$. It is easy to check that for all $\mathbf{w} \in \boldsymbol{\mathcal{W}}(K)$ the following equality holds

$$\mathrm{div}(\,\rho_K \mathbf{w}\,) \;=\; \pi_K\ (\mathrm{div}\,\mathbf{w}) \ . \tag{22}$$

Such property can also be expressed by the following commuting diagram

$$\begin{array}{ccc} \boldsymbol{\mathcal{W}}(K) & \xrightarrow{div} & L^2(K) \\ {\scriptstyle \rho_K}\downarrow & & \downarrow{\scriptstyle \pi_K} \\ \boldsymbol{\mathcal{M}}_k(K) & \xrightarrow{div} & \mathcal{D}_k(K) \end{array} \tag{23}$$

and it is in fact often called "commuting diagram property". At this point it is possible to prove the following result

Proposition 1.2. Let K be an affine element and ρ_K be the interpolation operator from $\boldsymbol{\mathcal{W}}(K)$ to $\boldsymbol{\mathcal{M}}_k(K)$. There exists a constant $c = c(k, K)$ such that

$$\|\,\mathrm{div}(\mathbf{w} \,-\, \rho_K \mathbf{w})\,\|_{0,K} \;\leq\; c\ {h_K}^m\,|\,\mathrm{div}\,\mathbf{w}\,|_{m,K} \qquad 1 \leq m \leq \phi(\mathcal{M}_k) \tag{24}$$

where

$$\phi(\mathcal{M}_k) = \begin{cases} k & \text{for } \mathcal{BDM}_k \\ k+1 & \text{for other choices of } \mathcal{M}_k \end{cases}$$

$\Diamond$

As a consequence, choosing $\mathcal{RT}_k$ or $\mathcal{BDFM}_{k+1}$ leads to the same accuracy in $\mathbf{H}(\mathrm{div}, K)$ as we have in $L^2(K; \mathbb{R}^n)$, while with $\mathcal{BDM}_k$ we lost one order of accuracy [cfr. Sec. 4.4]. It is also important to notice that what we stated holds only for affine elements.

We can now simply define a *global* interpolation operator from $\boldsymbol{\mathcal{W}}(\Omega) := \mathbf{H}(\mathrm{div}, \Omega) \cap L^s(\Omega; \mathbb{R}^n)$ (for a fixed $s > 2$) into $\boldsymbol{\mathcal{M}}_k(\Omega)$ as follows

$$\Pi_h \ :\ \boldsymbol{\mathcal{W}}(\Omega) \longrightarrow \boldsymbol{\mathcal{M}}_k(\Omega) \quad : \quad \mathbf{w} \longmapsto \Pi_h \mathbf{w}\,|_K \;=\; \rho_K(\mathbf{w}\,|_K) \tag{25}$$

where the apex h indicates that the operator is associated to the mesh $\mathcal{T}_h$. Again, if we define the following global counterpart of $\mathcal{D}_k(K)$

$$\mathcal{D}_k(\Omega) := \left\{ \; v \in L^2(\Omega) \;:\; v|_K \in \mathcal{D}_k(K) \; \right\} \tag{26}$$

and we denote with P_h the L^2-projection on $\mathcal{D}_k(\Omega)$, we have therefore the following commuting diagram:

$$\begin{array}{ccc} \boldsymbol{\mathcal{W}}(\Omega) & \xrightarrow{div} & L^2(\Omega) \\ {\scriptstyle \Pi_h}\downarrow & & \downarrow{\scriptstyle P_h} \\ \boldsymbol{\mathcal{M}}_k(\Omega) & \xrightarrow{div} & \mathcal{D}_k(\Omega) \end{array} \tag{27}$$

Note that the global diagram is obtained by the local one (23) simply by substituting the simplex K with the whole domain Ω and the local operator with the corresponding global ones. In particular, as one may expect for reasons of analogy between the local and global scales, the diagram implies that

$$\mathrm{div}(\,\boldsymbol{\mathcal{M}}_k(\Omega)\,) \;=\; \mathcal{D}_k(\Omega) \;. \tag{28}$$

Finally we have from Propositions (1.1) and (1.2) the following estimates for the global interpolation error

Proposition 1.3 (Global Interpolation Error)**.** Let $\{\mathcal{T}_h\}_{h>0}$ be a regular family of triangulations of Ω and let Π_h be defined as in (25). Then there exists a constant c independent of h such that

$$\|\,\mathbf{w} \,-\, \Pi_h\,\mathbf{w}\,\|_{0,\Omega} \;\le\; c\; h^m \;|\,\mathbf{w}\,|_{m,\Omega} \qquad 1 \le m \le k+1 \tag{29}$$

$$\|\,\mathrm{div}(\mathbf{w} \,-\, \Pi_h\,\mathbf{w})\,\|_{0,\Omega} \;\le\; c\; h^s \;|\,\mathrm{div}\,\mathbf{w}\,|_{s,\Omega} \qquad 1 \le s \le \phi(\mathcal{M}_k) \tag{30}$$

where

$$\phi(\mathcal{M}_k) = \begin{cases} k & \text{for } \mathcal{BDM}_k \\ k+1 & \text{for other choices of } \mathcal{M}_k \end{cases}$$

$\Diamond$

Moreover, in light of the error analysis we will address in Section 3, we give two fundamental properties of the interpolation operator

Lemma 1.1. The operator Π_h satisfies

$$\int_\Omega \mathrm{div}\,(\mathbf{w} \,-\, \Pi_h\,\mathbf{w})\; v \; d\mathbf{x} \;=\; 0 \qquad \forall\, \mathbf{w} \in \boldsymbol{\mathcal{W}}_k(\Omega) \quad \forall\, v \in \mathcal{P}_k^d(\Omega) \;. \tag{31}$$

Moreover

$$\operatorname{div}(\,\mathcal{BDM}_k\,(\Omega)\,) \;=\; \mathcal{P}^d_{k-1}\,(\Omega) \tag{32}$$

$$\operatorname{div}(\,\mathcal{RT}_k\,(\Omega)\,) \;=\; \mathcal{P}^d_{k}\,(\Omega) \tag{33}$$

$$\operatorname{div}\left(\mathcal{BDFM}_{k+1}\,(\Omega)\right) \;=\; \mathcal{P}^d_{k}\,(\Omega) \tag{34}$$

where $\mathcal{P}^d_k$ denote the space of piecewise discontinuous polynomial of degree $\leq k$, namely

$$\mathcal{P}^d_k\,(\Omega,\mathcal{T}_h) := \left\{\; v \in L^2\,(\Omega) \;:\; v\,|_K \in \mathcal{P}_k\,(K) \quad \forall\, K \in \mathcal{T}_h \;\right\}. \tag{35}$$

Proof. For brevity, let us consider the case of $\mathcal{RT}_k$. First, we rewrite the integral over the domain Ω by enhancing the contributions over the simplices, namely:

$$\int_\Omega \operatorname{div}\,(\mathbf{w} \,-\, \Pi_h\,\mathbf{w})\,v\;d\mathbf{x} \;=\; \sum_{K\in\mathcal{T}_h}\int_K \operatorname{div}\,(\mathbf{w} \,-\, \Pi_h\,\mathbf{w})\,v\;d\mathbf{x}\;.$$

We consider a single addend $\int_K$ for a fixed K and apply the Green's formula

$$\int_K \operatorname{div}\,(\mathbf{w} \,-\, \Pi_h\,\mathbf{w})\,v\;d\mathbf{x} \;=\; -\int_K (\mathbf{w} \,-\, \Pi_h\,\mathbf{w})\cdot\nabla v\;d\mathbf{x} \;+\; \int_K (\mathbf{w} \,-\, \Pi_h\,\mathbf{w})\cdot\mathbf{n}\;v\;d\sigma$$

Using (1.2) it follows that, for any $\mathbf{w} \in \boldsymbol{\mathcal{W}}_k\,(K)$ and $v \in \mathcal{P}_k\,(K)$, the two addends are identically zero:

$$\int_K \operatorname{div}\,(\mathbf{w} \,-\, \Pi_h\,\mathbf{w})\,v\;d\mathbf{x} \;=\; 0$$

Since the simplex K is arbitrary, the above equality implies (31).

It is easy to see that $\operatorname{div}\mathcal{RT}_k\,(\Omega) \subset \mathcal{P}^d_k\,(\Omega)$. In order to see the other inclusion we need the following result, that is fundamental in the analysis of mixed finite element approximations

Lemma 1.2. Let $\Omega \subset \mathbb{R}^n$ be a bounded domain. Given $f \in L^2\,(\Omega)$ there exists $\mathbf{v} \in H^1\,(\Omega;\mathbb{R}^n)$ such that

$$\operatorname{div}\mathbf{v} \;=\; f \qquad \text{in} \quad \Omega \tag{36}$$

and

$$\|\,\mathbf{v}\,\|_{H^1(\Omega;\mathbb{R}^n)} \;\leq\; C\;\|\,f\,\|_{0,\Omega} \tag{37}$$

with C constant depending only on Ω.

From Lemma 1.2 we know that $\operatorname{div} : H^1\,(\Omega;\mathbb{R}^n) \to L^2\,(\Omega)$ is surjective. Therefore, given $v \in \mathcal{P}^d_k\,(\Omega)$ there exists $\mathbf{w} \in H^1\,(\Omega;\mathbb{R}^n)$ such that $\operatorname{div}\,\mathbf{w} = v$. Then, it follows from (31) that $\operatorname{div}\,\Pi_h\,\mathbf{w} = v$ and so (32) is proved. ■

Note that, although we considered the particular case of the Raviart-Thomas spaces on simplicial elements, the proof only makes use of the fundamental commutative diagram property (27) and of the approximation properties of the operator Π_h. Therefore, the same argument holds for other choices of $\boldsymbol{\mathcal{M}}_k\,(\Omega)$, provided that we have a proper definition of the interpolation operator [cfr. (1.2)].

2 Mathematical Formulation of the Problem

2.1 Modelling Flow in Porous Media: Darcy's Law

We want to model the Fluid Dynamics of a porous medium occupying a region Ω. We assume that the fluid flow is laminar; we neglect the inertial effect in the fluid and only consider friction between the pores and the fluid. By neglecting also gravity, for simplicity, the Darcy law reads:

$$\mathbf{u} = -\,\mathbb{K}\,\nabla p\ , \tag{38}$$

where p is the pore pressure and $\mathbf{u}$ is the relative fluid flow vector in the tissue, given by $m(\mathbf{u}^f - \mathbf{u}^s)$, being m is the porosity, and $\mathbf{u}^f$ and $\mathbf{u}^s$ the Eulerian fluid and solid component velocities. The coefficient $\mathbb{K}$ represents the permeability tensor divided by the viscosity, i.e.,

$$\mathbb{K} = \frac{\hat{\mathbb{K}}}{\mu}\ , \tag{39}$$

where $\hat{\mathbb{K}}$ is the intrinsic permeability tensor and μ the viscosity of the fluid. We assume that $\mathbb{K}$ is bounded, symmetric and uniformly positive definite, i.e. there exists $\alpha \in \mathbb{R}^+$ such that

$$\boldsymbol{\xi}^T\ \mathbb{K}\,\boldsymbol{\xi}\ \geq\ \alpha\ \|\,\boldsymbol{\xi}\,\|^2 \qquad \forall \boldsymbol{\xi} \in \mathbb{R}^n\ . \tag{40}$$

When the constant gravity g is included, the relation between the velocity and pressure is expressed by

$$\mathbf{u} = -\,\mathbb{K}\,\nabla(p\ -\ \rho g z)\ ,$$

where $\rho > 0$ is the constant density and z the height. Moreover, we will often reduce to the simplest case of *isotropic* media whose permeability tensor is given $\mathbb{K} = \kappa\,\mathbb{I}$, being κ the scalar permeability and $\mathbb{I}$ the identity tensor. If this is the case, it is sufficient to require that $\kappa = \kappa(\mathbf{x})$ is a function bounded by above and below by positive constants. For instance, one may choose $\kappa \equiv \kappa_0/\mu > 0$.

2.2 Primal formulation

Two different mathematical formulations of the Darcy problem[2] are presented. Consider a bounded polygonal domain $\Omega \subset \mathbb{R}^n$ with $n = 2, 3$. We call *primal* or *divergence* form of the Darcy problem the following homogeneous Dirichlet boundary value problem for a second order elliptic PDE:

$$\begin{cases} -\ \mathrm{div}\ (\kappa\ \nabla p)\ =\ f & \text{in}\quad \Omega \\ \qquad\qquad\quad p\ =\ 0 & \text{on}\quad \partial\Omega \end{cases}\ , \tag{41}$$

where $\kappa = \kappa(\mathbf{x})$ is a function bounded by above and below by positive constants and $f \in L^2(\Omega)$ a sink or source term. The choice of boundary conditions is made for ease of

[2] We indicate with this term the coupling between (38) and the conservation of total mass.

presentation, since similar results are valid for other boundary conditions. The standard approach to address this problem is to find a weak solution of (41) in the following subspace of $H^1(\Omega)$

$$H_0^1(\Omega) := \left\{ \phi \in H^1(\Omega) \ : \ \phi = 0 \text{ on } \partial\Omega \right\}, \tag{42}$$

that is Hilbert space with respect to the standard H^1 norm $\| \cdot \|_{1,\Omega}^2 := \| \cdot \|_{0,\Omega}^2 + \| \nabla \cdot \|_{0,\Omega}^2$ or, equivalently, with the seminorm $| \cdot |_{1,\Omega} := \| \nabla \cdot \|_{0,\Omega}$. Then, the variational formulation of (41) requires to

Find $p \in H_0^1(\Omega)$ such that

$$\int_\Omega \kappa \, \nabla p \cdot \nabla q \, d\mathbf{x} \ = \ \int_\Omega f \, q \, d\mathbf{x} \qquad \forall \, q \in H^1(\Omega) \ . \tag{43}$$

Recall that (43) is commonly referred to as "homogeneous Dirichlet problem for the Poisson equation". Well-posedness of (43) easily follows from the application of *Friedrichs-Poincaré inequality* and the *Lax-Milgram lemma* (see for example [22]).

Therefore, in Section 3.1 we will propose different approaches to approximately solve the primal weak problem (43) within the context of Finite Element Methods (FEMs).

2.3 Mixed formulation

Nevertheless, in many applications one is mainly interested in the approximation of the velocity field, $\mathbf{u} = -\kappa \nabla p$, hence it could be desirable to solve the problem with respect to both the unknowns, $\mathbf{u}$ and p, simultaneously. Indeed, this is the fundamental idea of Mixed Finite Element methods (MFEM). With this purpose, problem (41) is decomposed into a first order system as follows:

$$\left\{ \begin{array}{rcll} \mathbf{u} \ + \ \kappa \nabla p & = & 0 & \text{in} \quad \Omega \\ \operatorname{div} \mathbf{u} & = & f & \text{in} \quad \Omega \\ p & = & 0 & \text{on} \quad \partial\Omega \end{array} \right. . \tag{44}$$

To write an appropriate weak formulation of this problem we introduce the space

$$\mathbf{H}(\operatorname{div}, \Omega) := \left\{ \mathbf{v} \in L^2(\Omega; \mathbb{R}^n) \ : \ \operatorname{div} \mathbf{v} \in L^2(\Omega) \right\}, \tag{45}$$

which is a Hilbert space with norm given by

$$\| \mathbf{v} \|_{\mathbf{H}(\operatorname{div},\Omega)}^2 := \| \mathbf{v} \|_{L^2(\Omega;\mathbb{R}^n)}^2 \ + \ \| \operatorname{div} \mathbf{v} \|_{L^2(\Omega)}^2 . \tag{46}$$

In order to derive the weak formulation, we start dividing by the non-zero function κ the first equation of (44) in order to gain a symmetric formulation of the mixed problem. Then,

multiplying the two equations by a vectorial test functions $\mathbf{v}$ and a scalar test function q, respectively, and integrating them over the domain Ω, we have

$$\int_\Omega \frac{1}{\kappa}\,\mathbf{u}\cdot\mathbf{v}\;d\mathbf{x} \;+\; \int_\Omega \nabla p\;\mathbf{v}\;d\mathbf{x} \;=\; 0\;, \tag{47}$$

$$\int_\Omega (\operatorname{div}\mathbf{u})\;q\;d\mathbf{x} \;=\; \int_\Omega f\,q\;d\mathbf{x}\;. \tag{48}$$

We apply the Green's formula to equation (47) to gain a skew-symmetric term, namely:

$$\int_\Omega \frac{1}{\kappa}\,\mathbf{u}\cdot\mathbf{v}\;d\mathbf{x} \;-\; \int_\Omega p\;(\operatorname{div}\mathbf{v})\;\;d\mathbf{x} \;+\; \int_{\partial\Omega} p\;\mathbf{v}\cdot\mathbf{n}\;d\sigma \;=\; 0\;, \tag{49}$$

$$\int_\Omega (\operatorname{div}\mathbf{u})\;q\;d\mathbf{x} \;=\; \int_\Omega f\,q\;d\mathbf{x}\;. \tag{50}$$

Finally, we enforce the boundary condition (44)(iii) at the level of the weak formulation. Indeed, it is well-known that in mixed formulations of boundary value problems the Dirichlet-type boundary condition is implicit in the weak formulation (i.e. it is the type of condition usually called *natural*). Instead, Neumann-type boundary conditions would have to be imposed on the space (*essential* conditions). This is exactly opposite to what happens in the case of standard formulations.

In the remainder, let us denote the Hilbert space for velocity with $\mathbf{V} \equiv \mathbf{H}(\operatorname{div},\Omega)$ and its norm with $\|\cdot\|_{\mathbf{V}}$ [cfr. (46)]. Similarly, for the pressure we define $Q \equiv L^2(\Omega)$ and $\|\cdot\|_Q \equiv \|\cdot\|_{0,\Omega}$. Moreover, we define the bilinear forms $a(\,\cdot\,,\,\cdot\,) : \mathbf{V}\times\mathbf{V} \longrightarrow \mathbb{R}^+$ and $b(\,\cdot\,,\,\cdot\,) : \mathbf{V}\times Q \longrightarrow \mathbb{R}^+$ by

$$a(\,\mathbf{u}\,,\,\mathbf{v}\,) \;=\; (\,\frac{1}{\kappa}\,\mathbf{u}\,,\,\mathbf{v}\,)_{0,\Omega}\;, \tag{51}$$

$$b(\,\mathbf{u}\,,\,q\,) \;=\; (\,\operatorname{div}\mathbf{u}\,,\,q\,)_{0,\Omega}\;, \tag{52}$$

where $(\,\cdot\,,\,\cdot\,)_{0,\Omega}$ indicates the inner product on $L^2(\Omega)$. Then the variational formulation of problem (44) is to

Find $(\mathbf{u},p) \in \mathbf{V}\times Q$ such that

$$\begin{cases} a(\,\mathbf{u}\,,\,\mathbf{v}\,) \;-\; b(\,\mathbf{v}\,,\,p\,) \;=\; 0 & \forall\,\mathbf{v}\in\mathbf{V} \\ \quad b(\,\mathbf{u}\,,\,q\,) \;=\; (\,f\,,\,q\,)_{0,\Omega} & \forall\,q\in Q \end{cases}\;. \tag{53}$$

Observe that the weak formulation (53) involves the divergence of the solution and of the test functions but not arbitrary first derivatives. This fact allows us to work on the space $\mathbf{H}(\operatorname{div},\Omega)$ instead of the smaller $H^1(\Omega;\mathbb{R}^n)$ and this will be important for the finite element approximation because piecewise polynomials vector functions do not need to have both components continuous to be in $\mathbf{H}(\operatorname{div},\Omega)$, but only their normal component as we will see in Section 3.2.

2.4 Well-posedness of the Mixed Formulation

To prove the existence and uniqueness of the solution of the variational problem (53), we employ the abstract theory on *Saddle Point Problems in Hilbert Spaces* developed in [6, 10].

First we fix the notational framework. We define the linear continuous operators associated with the bilinear forms $a(\cdot\,,\cdot\,)$ and $b(\cdot\,,\cdot\,)$, respectively, and their transposed counterparts. The linear operators $A : \mathbf{V} \longrightarrow \mathbf{V}'$ and $A^T : \mathbf{V} \longrightarrow \mathbf{V}'$ satisfies

$$\langle\, A\mathbf{u}\,,\,\mathbf{v}\,\rangle_{\mathbf{V}'\times\mathbf{V}} \;=\; a(\,\mathbf{u}\,,\,\mathbf{v}\,) \;=\; \big\langle\,\mathbf{u}\,,\,A^T\mathbf{v}\,\big\rangle_{\mathbf{V}\times\mathbf{V}'} \qquad \forall\,\mathbf{u}\in\mathbf{V} \quad \mathbf{v}\in\mathbf{V}\;. \tag{54}$$

Similarly, we define $B : \mathbf{V} \longrightarrow Q'$ and $B^T : Q \longrightarrow \mathbf{V}'$ by

$$\langle\, B\mathbf{v}\,,\,q\,\rangle_{Q'\times Q} \;=\; b(\,v\,,\,q\,) \;=\; \big\langle\,\mathbf{v}\,,\,B^Tq\,\big\rangle_{\mathbf{V}\times\mathbf{V}'} \qquad \forall\,\mathbf{v}\in\mathbf{V} \quad \forall\,q\in Q\;. \tag{55}$$

We also set

$$K \;\equiv\; \mathrm{Ker}\,B \;:=\; \big\{\;\mathbf{v}\in\mathbf{V}\;:\;b(\,v\,,\,q\,)=0 \quad \forall\,q\in Q\;\big\}\;, \tag{56}$$

$$H \;\equiv\; \mathrm{Ker}\,B^T := \big\{\;q\in Q\;:\;b(\,v\,,\,q\,)=0 \quad \forall\,\mathbf{v}\in\mathbf{V}\;\big\}\;. \tag{57}$$

For the well-posedness to be achieved we first require the following *continuity* assumption for the bilinear forms $a(\cdot\,,\cdot\,)$ and $b(\cdot\,,\cdot\,)$,

$$|\,a(\,\mathbf{u}\,,\,\mathbf{v}\,)\,| \;\le\; \|\,a\,\|\;\|\,\mathbf{u}\,\|_{\mathbf{V}}\,\|\,\mathbf{v}\,\|_{\mathbf{V}}\;, \tag{58}$$

$$|\,b(\,\mathbf{v}\,,\,q\,)\,| \;\le\; \|\,b\,\|\;\|\,\mathbf{v}\,\|_{\mathbf{V}}\,\|\,q\,\|_{Q}\;, \tag{59}$$

where $\|\,a\,\|$, $\|\,b\,\|$ indicate the norm of the continuous bilinear forms. For example, $\|\,b\,\|$ is defined as follows

$$\|\,b\,\| \;\equiv\; \|\,b\,\|_{\mathcal{L}(\mathbf{V}\times Q,\,\mathbb{R})} := \sup_{\mathbf{V}\times Q}\frac{b(\,\mathbf{v}\,,\,q\,)}{\|\,\mathbf{v}\,\|_{\mathbf{V}}\,\|\,q\,\|_{Q}}\;. \tag{60}$$

It is worth noting that the continuity of the three objects b, B, and B^T is just the same property. In particular we have

$$\|\,B\,\|_{\mathcal{L}(\mathbf{V}',\,Q)} \;=\; \|\,B^T\,\|_{\mathcal{L}(Q,\,\mathbf{V}')} \;=\; \|\,b\,\|_{\mathcal{L}(\mathbf{V}\times Q,\,\mathbb{R})}\;. \tag{61}$$

Moreover, note that problem (53) can also be written as

$$\left\{\begin{array}{rcll} A\mathbf{u} \;-\; B^Tp \;&=&\; 0 & \text{in}\quad \mathbf{V}' \\ B\mathbf{u} \;&=&\; f & \text{in}\quad Q' \end{array}\right.\;, \tag{62}$$

and from now on we shall consider the formulations (53) and (62) to be the same, referring to one or the other according to the convenience of the moment. We now want to find conditions implying existence and possibly uniqueness of solutions to this problem.

REMARK 1. If the bilinear form $a(\cdot\,,\cdot)$ is symmetric, the equations (53) are the optimality conditions of the minimisation problem

$$\inf_{B\mathbf{v}=f} \frac{1}{2}\, a(\,\mathbf{v}\,,\,\mathbf{v}\,)\ . \tag{63}$$

The variable p is then the Lagrange multiplier associated with the constraint $B\mathbf{v} = f$, and the associated saddle point problem is

$$\inf_{\mathbf{v}\in\mathbf{V}}\ \sup_{q\in Q}\ \frac{1}{2}\, a(\,\mathbf{v}\,,\,\mathbf{v}\,)\ +\ b(\,\mathbf{v}\,,\,q\,)\ -\ \langle\, f\,,\,q\,\rangle_{Q'\times Q}\ . \tag{64}$$

Indeed, this is the reason for the name of this analysis, in spite of the fact that we deal in fact with a more general case. Moreover, we would like to mention that the whole theory we develop here, for saddle point problems of the form (62), could be easily extended to similar problems with an additional right hand side in the first equation, namely $g \in \mathbf{V}'$. In such case we would add a term $-\langle\, g\,,\,\mathbf{v}\,\rangle_{\mathbf{V}'\times\mathbf{V}}$ to both equations (63) and (64). □

It is clear from the second equation of (62) that, in order to have existence of a solution for every $f \in Q'$, we must have $\mathrm{Im}B = Q'$. Finally, we state the following

Theorem 2.1 (EXISTENCE AND UNIQUENESS FOR SADDLE POINT PROBLEMS)**.** If the bilinear forms $a(\cdot\,,\cdot)$ and $b(\cdot\,,\cdot)$ are continuous and

$$(i)\quad \mathrm{Im}B = Q'\ , \tag{65}$$

$$(ii)\quad \exists\,\alpha_0 > 0\ :\ a(\,\mathbf{v}_0\,,\,\mathbf{v}_0\,)\ \geq\ \alpha_0\,\|\,\mathbf{v}_0\,\|^2_{\mathbf{V}} \qquad \forall\,\mathbf{v}_0 \in K\ , \tag{66}$$

then, for every $f \in Q'$, problem (53) has a unique solution. ◊

A proof of the theorem can be found for instance in [10, 3].

REMARK 2. Property (77) expresses the coercivity of $a(\cdot\,,\cdot)$ on the null-space K. Observe that it may hold while there is no coercivity on $\mathbf{V}$. □

It is important to observe that Theorem 2.1 does not give a necessary and sufficient condition. To get it, we must weaken the coercivity condition (77). The most general results is obtained by restricting the bilinear form $a(\cdot\,,\cdot)$ to K and considering the two operators $A_{KK'}$, $A^T_{KK'}$. It may be proved (see [10, 3]) that the two following conditions are necessary and sufficient for the problem (53) to be uniquely solvable:

$$(i)\quad \mathrm{Im}B = Q'\ , \tag{67}$$

$$(ii)'\ A_{KK'} \text{ is an isomorphism from } K \text{ to } K'\ . \tag{68}$$

For brevity we skip the details that would require several results of Functional Analysis. Instead, we prefer to express conditions (67) and (68) in a different way, to emphasize the role of the stability constants.

Let us start from condition (67). According to a note Corollary of the *Banach Closed Range Theorem*, we know that it holds if and only if the operator B^T is bounding, that is, if and only if

$$\exists\, \beta > 0 \quad \text{s.t.} \quad \| B^T q \|_{\mathbf{V}'} \geq \beta \, \| q \|_Q \qquad \forall\, q \in Q \; . \tag{69}$$

We now want to define, somehow, the best possible constant that would fit in (69). For this, we note that it is equivalent to

$$\inf_{q \in Q} \frac{\| B^T q \|_{\mathbf{V}'}}{\| q \|_Q} \; \geq \; \beta \; ,$$

which, recalling the definition of norm in a dual space and (55), becomes

$$\beta \; \leq \; \inf_{q \in Q} \; \sup_{\mathbf{v} \in \mathbf{V}} \; \frac{b(\, \mathbf{v} \, , \, q \,)}{\| \, \mathbf{v} \, \|_{\mathbf{V}} \, \| \, q \, \|_Q} \tag{70}$$

which is possibly the most commonly used among the many equivalent formulations of assumption (67) and it is usually referred to as *inf-sup condition* on $b(\,\cdot\,,\,\cdot\,)$. With similar arguments, we see that condition (68) is equivalent to saying that there exists an $\alpha_1 > 0$ such that

$$\begin{aligned} \alpha_1 \; &\leq \; \inf_{\mathbf{v}_0 \in K} \; \sup_{\mathbf{w}_0 \in K} \; \frac{a(\, \mathbf{v}_0 \, , \, \mathbf{w}_0 \,)}{\| \, \mathbf{v}_0 \, \|_{\mathbf{V}} \, \| \, \mathbf{w}_0 \, \|_{\mathbf{V}}} \; , \\ \alpha_1 \; &\leq \; \inf_{\mathbf{v}_0 \in K} \; \sup_{\mathbf{w}_0 \in K} \; \frac{a(\, \mathbf{v}_0 \, , \, \mathbf{w}_0 \,)}{\| \, \mathbf{v}_0 \, \|_{\mathbf{V}} \, \| \, \mathbf{w}_0 \, \|_{\mathbf{V}}} \; , \end{aligned} \tag{71}$$

which is called *double-inf-sup condition* on the restriction of $a(\,\cdot\,,\,\cdot\,)$ on K.

Remark 3. Note that we are assuming implicitly that for fractions of the type $l(v)/\| \, v \, \|_V$ with $l(\cdot)$ linear functional on a Banach space V, the supremum and the infimum are taken for $v \neq 0$, and therefore we write the supremum (or infimum) for $v \in V$ rather than for $v \in V \setminus 0$. □

Finally, we here the following final result that is, in some sense, a generalization of Lax-Milgram lemma for saddle point problems and could be considered as the main result of this section

Theorem 2.2. [Stability Estimates for Saddle Point Problems] Assume the bilinear forms $a(\,\cdot\,,\,\cdot\,)$ and $b(\,\cdot\,,\,\cdot\,)$ are continuous and there exist two positive constant α_1 and β such that the conditions (71)-(70) are satisfied.

Then, for every $f \in Q'$, problem (53) has a unique solution that is bounded by

$$\| \, \mathbf{u} \, \|_{\mathbf{V}} \; \leq \; \frac{2 \| \, a \, \|}{\alpha_1 \, \beta} \; \| \, f \, \|_{Q'} \; , \tag{72}$$

$$\| \, p \, \|_Q \; \leq \; \frac{2 \| \, a \, \|^2}{\alpha_1 \, \beta^2} \; \| \, f \, \|_{Q'} \; . \tag{73}$$

If, moreover, $a(\,\cdot\,,\,\cdot\,)$ is symmetric and *positive*,

$$a(\,\mathbf{v}\,,\,\mathbf{v}\,) \geq 0 \qquad \forall\, \mathbf{v} \in \mathbf{V}, \tag{74}$$

then we have the improved estimates

$$\|\,\mathbf{u}\,\|_{\mathbf{V}} \;\leq\; \frac{2\|\,a\,\|^{1/2}}{\alpha_0^{1/2}\,\beta}\;\|\,f\,\|_{Q'}\;, \tag{75}$$

$$\|\,p\,\|_{Q} \;\leq\; \frac{\|\,a\,\|}{\beta^2}\;\|\,f\,\|_{Q'}\;, \tag{76}$$

where α_0 is the constant appearing in (77). $\Diamond$

Equations (72)-(73) (or, equivalently, (75)-(76)) are called *stability estimates* because they show the norm of the solution $(\mathbf{u},\, p)$ of (53) can be bounded in terms of the norms of the datum f, together with the values of the constants α and β and the norm $\|\,a\,\|$ of the bilinear form a. Moreover, we have that, if the bilinear form $a(\,\cdot\,,\,\cdot\,)$ is coercive on the whole space, namely

$$\exists\, \alpha > 0 \;:\; a(\,\mathbf{v}\,,\,\mathbf{v}\,) \;\geq\; \alpha\,\|\,\mathbf{v}\,\|^2_{\mathbf{V}} \qquad \forall\, \mathbf{v} \in \mathbf{V}\;, \tag{77}$$

then it holds a useful corollary with identical statement than Theorem (2.2) but with the constant α replacing both α_1 and α_0.

Remark 4. In the case of saddle point problems with an additional right hand side $g \in \mathbf{V}'$ in the fist equation, as mentioned in Remark 1, the above statements have to be modified by adding a term proportional to $\|\,g\,\|_{\mathbf{V}'}$ in all the estimates. $\square$

Finally, to achieve the well-posedness in the particular case of mixed Darcy we have to verify that bilinear forms (51), (52) satisfy the above assumptions. We have that B is the divergence operator from $\mathbf{H}\,(\mathrm{div}, \Omega)$ into $L^2\,(\Omega)$. It is not difficult to check that it is surjective: for instance, we can use the fact that the primal variational formulation (43) has a unique solution thanks to the Lax-Milgram lemma. The kernel of B is

$$K \equiv \left\{\; \mathbf{v}_0 \in \mathbf{H}\,(\mathrm{div}, \Omega) \;:\; \mathrm{div}\,\mathbf{v}_0 = 0 \;\right\}\;, \tag{78}$$

and it is easy to prove that $a(\,\cdot\,,\,\cdot\,)$ is coercive on K (although it is *not coercive* on $\mathbf{H}\,(\mathrm{div}, \Omega)$), thanks to the assumption of uniform boundedness of the permeability $\kappa(\mathbf{x})$. Our abstract theory applies immediately, and we have existence and uniqueness of the solution.

3 Finite Element Approximation

In this Section we propose some Galerkin-FEM approximations to both (41) and (44). Assume for the remainder that $\Omega \subset \mathbb{R}^n$ is a polygonal (resp. polyhedronal) bounded Lipschitz domain and $\mathcal{T}_h$ is a shape-regular triangulation of Ω into closed triangles (resp. tetrahedrons) with size $\mathcal{O}(h)$, for $n = 2$ $(n = 3)$.

3.1 Finite Element approximations of the primal problem

Before focusing on the mixed finite element approximation of the problem, we recall two popular *classical* finite element methods for the numerical solution of (41). The idea is to derive the general Galerkin-FEM approximation of the problem and then to propose two possible choices of the approximation spaces. A comparison of the methods under consideration, together with the mixed ones proposed in 3.2, is also provided in 3.3.

We apply the Galerkin method [22] to obtain approximate solutions of (43) by "projecting" the variational problem on proper finite-dimensional subspaces of $V := H_0^1(\Omega)$. Let $\{V_h \mid h \geq 0\}$ be a sequence of subspaces of V with the following "approximation property",

$$\overline{\bigcup_{h>0} V_h} \equiv V \ , \tag{79}$$

being h an index that is inversely proportional to the (finite) dimension of each subspace, N_h. Let $\{\psi_i\}_{i=1}^{N_h}$ be a basis in V_h. To realize the projection, we look for an approximation of the solution $p \in V$ in the form

$$p_h(\mathbf{x}) = \sum_{j=1}^{N_h} p_j \, \psi_j(\mathbf{x}) \ . \tag{80}$$

The Galerkin formulation of (43) is hence obtained by simply adding the apex h, namely:

Given $f \in L^2(\Omega)$, find $p_h \in V_h$ such that $p_h = 0$ on $\partial\Omega$ and

$$\int_\Omega \kappa \, \nabla p_h \cdot \nabla q_h \, d\mathbf{x} \ = \ \int_\Omega f \, q_h \, d\mathbf{x} \qquad \forall \, q_h \in V_h \tag{81}$$

Note that the Dirichlet boundary condition (41)(b) has to be enforced directly on the numerical solution. The imposition of essential boundary conditions at the numerical level is a classical topic in Numerical Analysis and we refer to [21] for a detailed discussion. Moreover, it is possible to make a further step by substituting (80) in the variational problem (81) and by choosing $q = \psi_i$ for a fixed i, to rewrite the problem as a proper linear system. We postpone the discussion of the algebraic aspects to the case of specific finite element methods.

In the remainder, we will give two different finite element formulations of (43), obtained by solving (81) for two specific choices of the family $\{V_h\}$ (and the corresponding basis functions). The best-known and most widely used family of finite element methods relies on the definition of the the so-called *Lagrange* finite elements, whose degrees of freedom are simply identified as the point-wise evaluation of the unknown at an array of points (See Figure ?? a). We define for $k \geq 1$ the space

$$\mathcal{C}_k^0(\Omega, \mathcal{T}_h) := \mathcal{P}_k(\Omega, \mathcal{T}_h) \cap H_0^1(\Omega) \tag{82}$$

For both historical and practical reasons (we already used the usual symbol $\mathcal{P}_k$ for standard piece-wise polynomials) we named those spaces after the German mathematician Richard Courant. In fact, according to [24], in the early 1960s it was found that the method was an independent rediscovery of a simpler idea proposed in 1943 by Courant [12] for the lowest-order case $k = 1$. Finally, the *Courant* Finite Element Method (CFEM) reads:

Given $f \in L^2(\Omega)$, find $p_h^C \in \mathcal{C}_k^0(\Omega, \mathcal{T}_h)$ such that

$$\int_\Omega \kappa \, \nabla p_h^C \cdot \nabla q_h^C \, d\mathbf{x} \;=\; \int_\Omega f \, q_h^C \, d\mathbf{x} \qquad \forall \, q_h^C \in \mathcal{C}_k^0(\Omega, \mathcal{T}_h) \tag{83}$$

Note that a general function in $\mathcal{C}_k^0$ automatically belongs to the continuum space H_0^1. This is what we call a *conforming* finite element approximation of the solution of (41). Conversely, the second finite element method proposed by Crouzeix and Raviart [13] uses still piecewise polynomials, but unlike the Lagrange element, the degrees of freedom are located at edge midpoints rather than at vertices. This gives rise to a weaker form of continuity, but it is still a suitable C^0 nonconforming element. The extension to tetrahedra in $\mathbb{R}^3$ replaces the degrees of freedom on edge midpoints by degrees of freedom on face midpoints. See Figure ?? b for a graphic illustration. The corresponding *Crouzeix-Raviart* finite element spaces of order $k \geq 1$ reads

$$\mathcal{CR}_k^0(\Omega, \mathcal{T}_h) := \left\{ \; v_h \in \mathcal{P}_k^d(\Omega, \mathcal{T}_h) \;:\; [\, v_h \,]_{m,e} = 0 \quad \forall e \in \mathcal{E} \; \right\} \tag{84}$$

where the notation $[\,\cdot\,]_{m,e}$ indicates the function's generalized jump over the edge e, evaluated in correspondence of its midpoint. More precisely, if K_+ and K_- are the two simplices sharing the edge e (as in Fig.), we have

$$[\, v_h \,]_{m,e} = \begin{cases} v_h^+(\mathbf{x}_{m,e}) \;-\; v_h^-(\mathbf{x}_{m,e}) & \text{if} \quad e \in \mathcal{E} \setminus \partial\Omega \\ 0 & \text{if} \quad e \in \partial\Omega \end{cases} \tag{85}$$

being $\mathbf{x}_{m,e}$ the midpoint of edge e and $v_h^+ = v_h\,|_{K_+}$, $v_h^- = v_h\,|_{K_-}$. For example, a function in $\mathcal{CR}_1^0$ is uniquely determined by its value on $n+1$ points. Therefore, the derivation of a finite element approximation from (84) is not straightforward because $\mathcal{CR}_k^0 \not\subseteq H^1(\Omega)$. For this purpose we define the so-called *piecewise* gradient $\nabla_h \,:\, \mathcal{P}_k^d(\Omega) \longrightarrow \mathcal{P}_{k-1}^d(\Omega; \mathbb{R}^n)$ with

$$(\nabla_h \, v_h)\,|_K = \nabla\,(\, v_h\,|_K) \qquad \forall v_h \in \mathcal{CR}_k^0(\Omega, \mathcal{T}_h) \tag{86}$$

Therefore, the *Crouzeix-Raviart* Nonconforming Finite Element Method (CR-NCFEM) reads:

Given $f \in L^2(\Omega)$, find $p_h^{CR} \in \mathcal{CR}_k^0(\Omega, \mathcal{T}_h)$ such that

$$\int_\Omega \kappa \, \nabla_h \, p_h^{CR} \cdot \nabla_h \, q_h^{CR} \, d\mathbf{x} \;=\; \int_\Omega f \, q_h^{CR} \, d\mathbf{x} \qquad \forall \, q_h^{CR} \in \mathcal{CR}_k^0(\Omega, \mathcal{T}_h) \tag{87}$$

In conclusion, the nonconforming finite element method (87) appears to be more attractive than the conforming method (83) which involves more degrees of freedom without improving the asymptotic order of accuracy, as proved in [13].

3.2 Finite Element Approximations of the mixed problem

Let $\{\mathbf{V}_h \mid h \geq 0\}$ and $\{Q_h \mid h \geq 0\}$ denote two families of finite dimensional subspace of $\mathbf{H}(\mathrm{div}, \Omega)$ and $L^2(\Omega)$, respectively, fulfilling the usual approximation property (79). The Galerkin approximation to (44) reads:

Given $f \in L^2(\Omega)$, find $(\mathbf{u}_h, p_h) \in \mathbf{V}_h \times Q_h$ such that

$$\left\{ \begin{array}{rl} a(\,\mathbf{u}_h\,,\,\mathbf{v}_h\,) \,-\, b(\,\mathbf{v}_h\,,\,p_h\,) \;=\; 0 & \quad \forall\, \mathbf{v}_h \in \mathbf{V}_h \\ b(\,\mathbf{u}_h\,,\,q_h\,) \;=\; (\,f\,,\,q_h\,)_{0,\Omega} & \quad \forall\, q_h \in Q_h \end{array} \right. \tag{88}$$

where the bilinear forms $a(\,\cdot\,,\,\cdot\,)$ and $b(\,\cdot\,,\,\cdot\,)$ are defined as those in (**??**). Therefore, the Mixed Finite Element approximation of the problem is to choose the finite spaces $\mathbf{V}_h$, Q_h as proper finite elements spaces. Specifically, we approximate the velocity field by conforming elements of $\mathbf{H}(\mathrm{div}, \Omega)$, such as Raviart-Thomas (RT), Brezzi-Douglas-Marini (BDM), and Brezzi-Douglas-Fortin-Marini (BDFM) elements, and approximate the pressure by discontinuous polynomials of appropriate degrees. We have the following pair of spaces for $k \geq 1$

$$\mathbf{V}_h \;=\; \boldsymbol{\mathcal{M}}_k(\Omega, \mathcal{T}_h) \qquad Q_h \;=\; \mathcal{P}^d_{k-1}(\Omega, \mathcal{T}_h) \tag{89}$$

where $\boldsymbol{\mathcal{M}}_k$ and $\mathcal{P}^d_k$ are defined as in (13) and (35), respectively. Observe that, since no derivative of the scalar variable appears in the weak form, we do not require any continuity in the approximation space for the pressure. Specifically, the *Raviart-Thomas* Mixed Finite Element Method (RT-MFEM) reads:

Find $\left(\mathbf{u}_h^{RT}, p_h^{RT}\right) \in \mathcal{RT}_k(\Omega; \mathcal{T}_h) \times \mathcal{P}^d_k(\Omega; \mathcal{T}_h)$ for $k \geq 0$ such that

$$\left\{ \begin{array}{rl} a(\,\mathbf{u}_h^{RT}\,,\,\mathbf{v}_h\,) \,-\, b(\,\mathbf{v}_h\,,\,p_h^{RT}\,) \;=\; 0 & \quad \forall\, \mathbf{v}_h \in \mathcal{RT}_k(\Omega; \mathcal{T}_h) \\ b(\,\mathbf{u}_h^{RT}\,,\,q_h\,) \;=\; (\,f\,,\,q_h\,)_{0,\Omega} & \quad \forall\, q_h \in \mathcal{P}^d_k(\Omega; \mathcal{T}_h) \end{array} \right. \tag{90}$$

Similarly, the *Brezzi-Douglas-Marini* Mixed Finite Element Method (BDM-MFEM) reads:

Find $\left(\mathbf{u}_h^{BDM}, p_h^{BDM}\right) \in \mathcal{BDM}_{k+1}(\Omega; \mathcal{T}_h) \times \mathcal{P}^d_k(\Omega; \mathcal{T}_h)$ for $k \geq 0$ such that

$$\left\{ \begin{array}{rl} a(\,\mathbf{u}_h^{BDM}\,,\,\mathbf{v}_h\,) \,-\, b(\,\mathbf{v}_h\,,\,p_h^{BDM}\,) \;=\; 0 & \quad \forall\, \mathbf{v}_h \in \mathcal{BDM}_{k+1}(\Omega; \mathcal{T}_h) \\ b(\,\mathbf{u}_h^{BDM}\,,\,q_h\,) \;=\; (\,f\,,\,q_h\,)_{0,\Omega} & \quad \forall\, q_h \in \mathcal{P}^d_k(\Omega; \mathcal{T}_h) \end{array} \right. \tag{91}$$

Let us omit in the remainder the case BDFM since none of the usual finite element solvers implements those spaces.

3.3 Comparison and error analysis

The aim of this section is to establish a relationship between the four main finite element methods presented above, namely CFEM and CR-NCFEM for the primal form, RT-MFEM and BDM-MFEM for the mixed form. For the sake of simplicity, let us neglect the effect of the permeability of the medium, i.e. $k \equiv 1$.

A comparison of CFEM, CR-NCFEM, and RT-MFEM has been initiated in [4] and completed by C. Carstensen, D. Peterseim and M. Schedensack in [11]. The authors establish the equivalence of the conforming Courant finite element method, the nonconforming Crouzeix–Raviart finite element method, and several first-order discontinuous Galerkin finite element methods in the sense that the respective energy error norms are equivalent up to generic constants and higher-order data oscillations in a Poisson model problem. The Raviart–Thomas mixed finite element method is proved to be better than the previous methods.

Braess in [4] applied the *hypercircle method* to derive an a posteriori error estimator for the nonconforming P_1 element. The estimates lead, indeed, to a comparison of the nonconforming finite element solution with other finite element methods. The hypercircle method, also called the *two energies principle*, is based on the theorem of Prager and Synge (see [20]):

Theorem 3.1 (HYPERCIRCLE METHOD)**.** Let $\mathbf{u} \in \mathbf{H}(\mathrm{div}, \Omega)$, $q \in H_0^1(\Omega)$ and assume that

$$\mathrm{div}\, \mathbf{u} + f = 0 \,. \tag{92}$$

If p is the solution of

$$\left\{ \begin{array}{rcll} -\Delta p & = & f & \text{in} \quad \Omega \\ p & = & 0 & \text{on} \quad \partial\Omega \end{array} \right. , \tag{93}$$

then,

$$\| \nabla p - \nabla q \|^2 + \| \nabla p - \mathbf{u} \|^2 = \| \nabla q - \mathbf{u} \|^2 \,. \tag{94}$$

Proof. By applying Green's formula and noting that $\Delta p = \mathrm{div}\, \mathbf{u} = -f$ we have

$$\begin{aligned} \int_\Omega \nabla(p - q)(\nabla p - \mathbf{u})\, d\mathbf{x} = - \int_\Omega (p - q)(\Delta p - \mathrm{div}\, \mathbf{u})\, d\mathbf{x} \\ + \int_{\partial\Omega} (p - q) \left(\frac{\partial p}{\partial n} - \mathbf{u} \cdot \mathbf{n} \right) ds = 0 \end{aligned} \tag{95}$$

The boundary term above vanishes, since $p - q = 0$ on $\partial\Omega$. This orthogonality relation and the Pythagorean rule yield (94). ■

Obviously, the estimates can be used for finite element solution $q = p_h \in H^1(\Omega)$ as well as for a solution $\mathbf{u}_h \in \mathbf{H}(\mathrm{div}, \Omega)$ of a mixed method.

Let us now exploit the connection with the mixed method of Raviart and Thomas. For convenience, we restrict ourselves to the case that f is piecewise constant on the actual triangulation. Since $\mathrm{div}\,\mathbf{u} \in \mathcal{P}_k^d$, the relation $\mathrm{div}\,\mathbf{u} + f = 0$ holds pointwise. Marini [17] observed that the Raviart–Thomas finite element solution $(\mathbf{u}_h^{RT}, p_h^{RT})$ can be obtained from the Crouzeix–Raviart FE solution on the same triangulation:

$$\mathbf{u}_h^{RT} = \nabla_h p_h^{CR} - \frac{1}{2} f_K(\mathbf{x} - \mathbf{x}_K), \qquad \mathbf{x} \in K\ , \tag{96}$$

$$p_h^{RT} = \frac{1}{|K|} \int_K \left[p_h^{CR} + \frac{1}{4} f_K(\mathbf{z} - \mathbf{x}_K) \cdot (\mathbf{z} - \mathbf{x}_K) \right] d\mathbf{z}, \qquad \mathbf{x} \in K\ , \tag{97}$$

where $f_K := {}^1\!/_{|K|} \int_K f\ d\mathbf{x}$ and $\mathbf{x}_K$ denotes the centroid of the element K.

There is not only the algebraic relation (96),(97) between the Crouzeix–Raviart element and the Raviart–Thomas element. Braess proved that errors of the solutions are also related:

Theorem 3.2 (COMPARATIVE ERROR ESTIMATES)**.** Let $p \in H_0^1(\Omega)$ be the exact solution of (93) and let p_h^{C1}, p_h^{C2} be the approximated solutions with linear and quadratic Courant finite elements, respectively. If f is piecewise constant, then

$$\| \nabla(p - p_h^{C2}) \| \leq \| \nabla p - \mathbf{u}_h^{RT} \| \leq \| \nabla(p - p_h^{CR}) \| \leq \| \nabla(p - p_h^{C1}) \|\ . \tag{98}$$

$\Diamond$

The relations in (98) are understood as inequalities modulo generic constants. A preference for the result of the Raviart-Thomas element is consistent with the comparison result.

4 Numerical Examples

Here we present some numerical benchmarks to illustrate the comparison between different finite element methods for the numerical solutions of (41) and (44), presented in the previous Section. We aim to prove that performances of our finite element solver are in agreement with the analytical result (98).

4.1 Available data

For the sake of simplicity, we assume the permeability of the porous medium to be isotropic: $\mathbb{K} = \kappa\, \mathbb{I}$. Moreover, we ignore the gravity component and we enforce homogeneous Dirichlet conditions over the whole boundary $\partial\Omega$. Indeed, the Darcy's problem in such a simplified

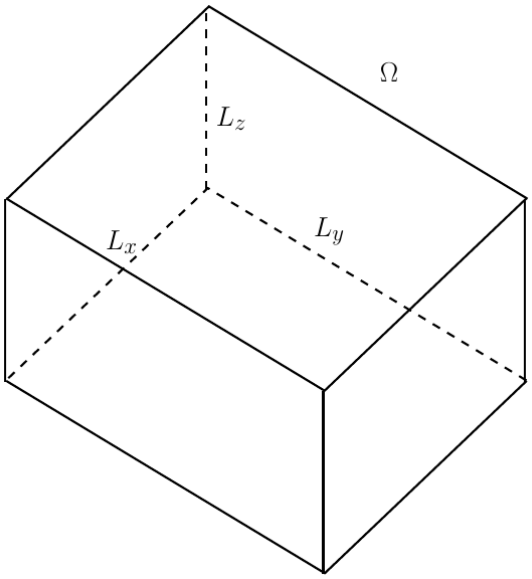

Figure 2: Computational domain for the numerical tests.

setting reads:

$$\begin{cases} \mathbf{u} + \kappa \nabla p = 0 & \text{in} \quad \Omega \\ \operatorname{div} \mathbf{u} = f & \text{in} \quad \Omega \\ p = 0 & \text{on} \quad \partial\Omega \end{cases} . \tag{99}$$

Equivalently, we have the *primal* or *pressure* formulation:

$$\begin{cases} \operatorname{div} (-\kappa \nabla p) = f & \text{in} \quad \Omega \\ p = 0 & \text{on} \quad \partial\Omega \end{cases} . \tag{100}$$

The domain under consideration is a parallelepiped in $\mathbb{R}^3$, namely $\Omega = [\,0, L_x\,] \times [\,0, L_y\,] \times [\,0, L_z\,]$, as shown in Fig. 2. An exact pressure solution for this simplified setting can be computed by hand, namely:

$$p(\mathbf{x}) = \sin\left(\frac{2\,\pi\,x}{L_x}\right) \sin\left(\frac{2\,\pi\,y}{L_y}\right) \sin\left(\frac{2\,\pi\,z}{L_z}\right) \ , \tag{101}$$

that evidently fulfils the boundary condition. The related velocity field follows from Darcy's law:

$$\mathbf{u}(\mathbf{x}) = -\kappa\,\nabla p(\mathbf{x}) = -2\pi\kappa \begin{bmatrix} \dfrac{1}{L_x}\,\cos\left(\dfrac{2\,\pi\,x}{L_x}\right)\sin\left(\dfrac{2\,\pi\,y}{L_y}\right)\sin\left(\dfrac{2\,\pi\,z}{L_z}\right) \\ \dfrac{1}{L_y}\,\sin\left(\dfrac{2\,\pi\,x}{L_x}\right)\cos\left(\dfrac{2\,\pi\,y}{L_y}\right)\sin\left(\dfrac{2\,\pi\,z}{L_z}\right) \\ \dfrac{1}{L_z}\,\sin\left(\dfrac{2\,\pi\,x}{L_x}\right)\sin\left(\dfrac{2\,\pi\,y}{L_y}\right)\cos\left(\dfrac{2\,\pi\,z}{L_z}\right) \end{bmatrix} . \tag{102}$$

Finally, we substitute the expression (102) into the mass equation to obtain the datum:

$$f(\mathbf{x}) = \nabla\cdot\mathbf{u}(\mathbf{x}) = 4\pi^2\kappa\,\left(\frac{1}{L_x^2}+\frac{1}{L_y^2}+\frac{1}{L_z^2}\right)p(\mathbf{x})\ . \tag{103}$$

In the remainder we will enforce the datum (103) within the computational solver and we will then compare the numerical solutions with (101), (102).

Figure 3 shows the exact solutions (101), (102), (103) on the simpler two-dimensional domain $\Omega = [\,0,1\,]^2$.

4.2 *FreeFem++* implementation

We implement a finite element solver for (99), (100) using *FreeFem++*, a partial differential equation solver with its own language [15]. In particular, we assemble the four finite element methods presented in 3.1, 3.2 on a generic domain $\Omega \subset \mathbb{R}^2$, namely:

- CFEM (83): conforming Courant/Lagrange method, $\mathcal{C}_k^0\,(\Omega)$
- CR-NCFEM (87): nonconforming Crouzeix-Raviart method, $\mathcal{CR}_{k+1}^0\,(\Omega)$
- RT-MFEM (90): H(div)-conforming Raviart-Thomas mixed method, $\left(\mathcal{RT}_k\,(\Omega)\,,P_k^d(\Omega)\right)$
- BDM-MFEM (91): H(div)-conforming Brezzi-Douglas-Marini mixed method, $\left(\mathcal{BDM}_{k+1}\,(\Omega)\,,P_k^d(\Omega)\right)$

of order $k \geq 0$. For simplicity, we present the two-dimensional version ($d = 2$) of the finite element formulations (83), (87), (90), (91). A visual comparison of the characteristic degrees of freedom for the 6 finite element method available in *FreeFem++* is given in figures 4, 5. Numerical results are given in Sec. 4.3.

For further details about the implementation see Sec. A.

4.3 Primal and mixed numerical results

We apply the finite element solver to simulate the benchmark problem described in Sec. 4.1 for the six different configurations provided in Sec. 4.2. The computational domain is represented in Fig. 6.

a

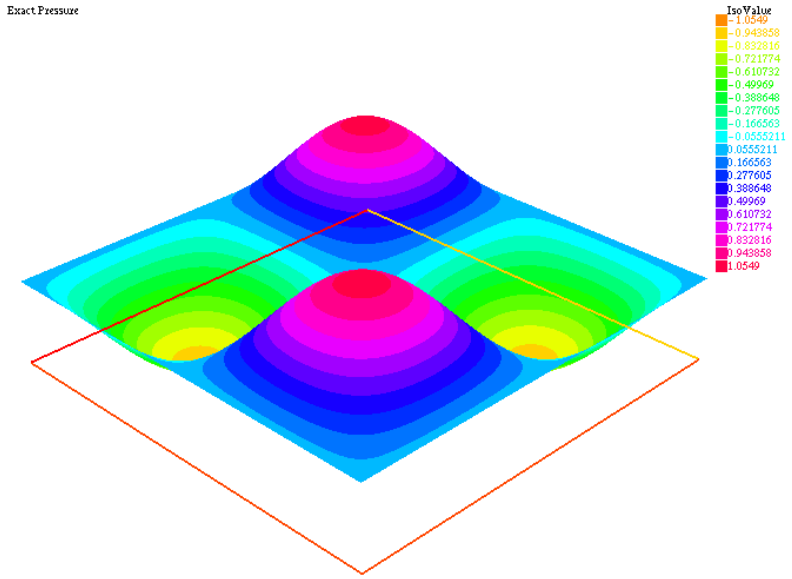
Exact Pressure
IsoValue
-1.0549
-0.943858
-0.832816
-0.721774
-0.610732
-0.49969
-0.388648
-0.277605
-0.166563
-0.0555211
0.0555211
0.166563
0.277605
0.388648
0.49969
0.610732
0.721774
0.832816
0.943858
1.0549

b

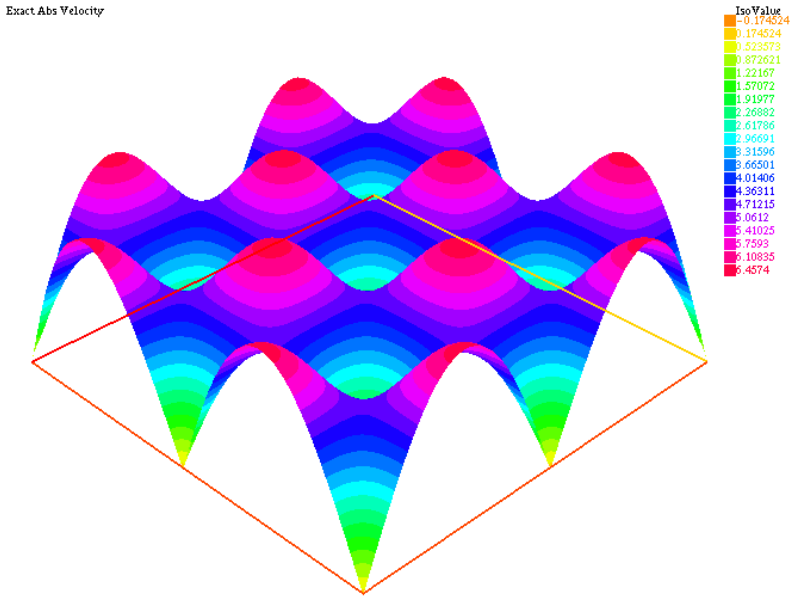
Exact Abs Velocity
IsoValue
0.174524
0.523573
0.872621
1.22167
1.57072
1.91977
2.26882
2.61786
2.96691
3.31596
3.66501
4.01406
4.36311
4.71215
5.0612
5.41025
5.7593
6.10835
6.4574

c

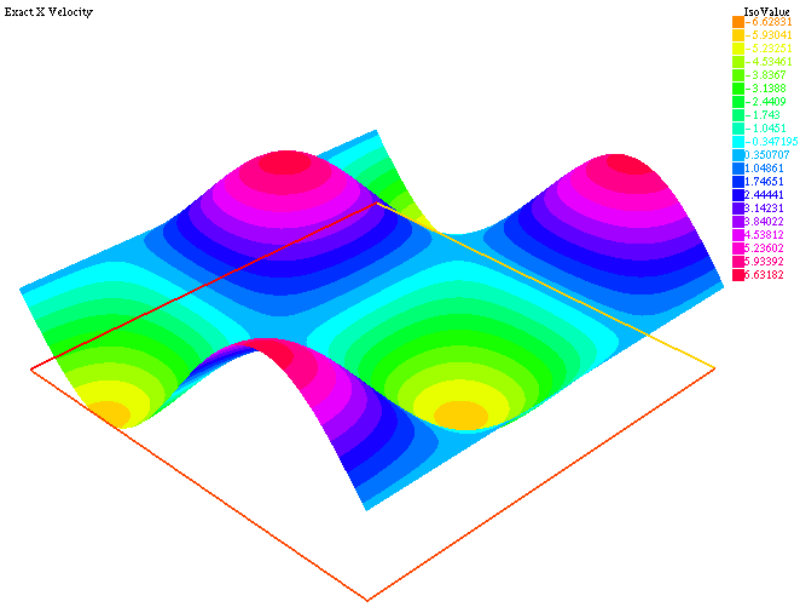

d

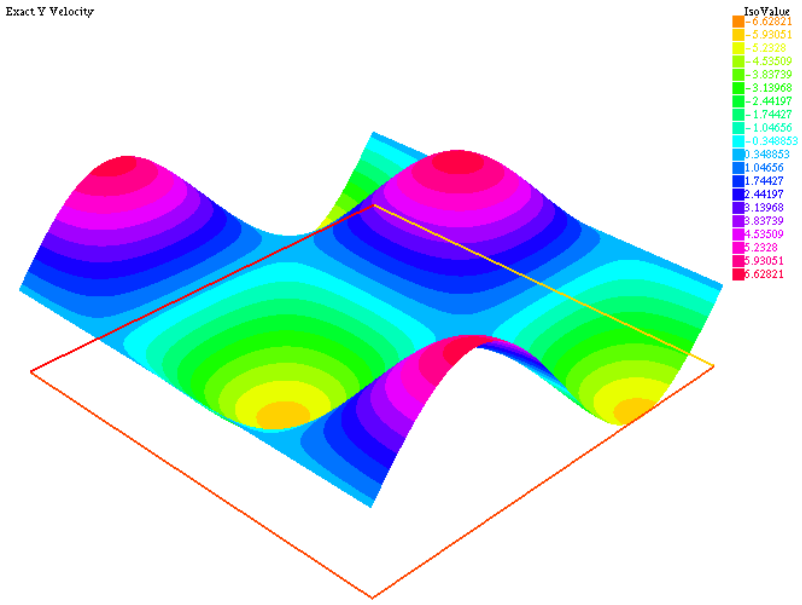

Figure 3: Exact solution of the Darcy's problem (99) on $\Omega = [0,1]^2$. Proceeding from top-left to bottom-right: (a) the exact pressure p, (b) the exact velocity magnitude $|\mathbf{u}|$, (c), (d) the X and Y components of $\mathbf{u}$.

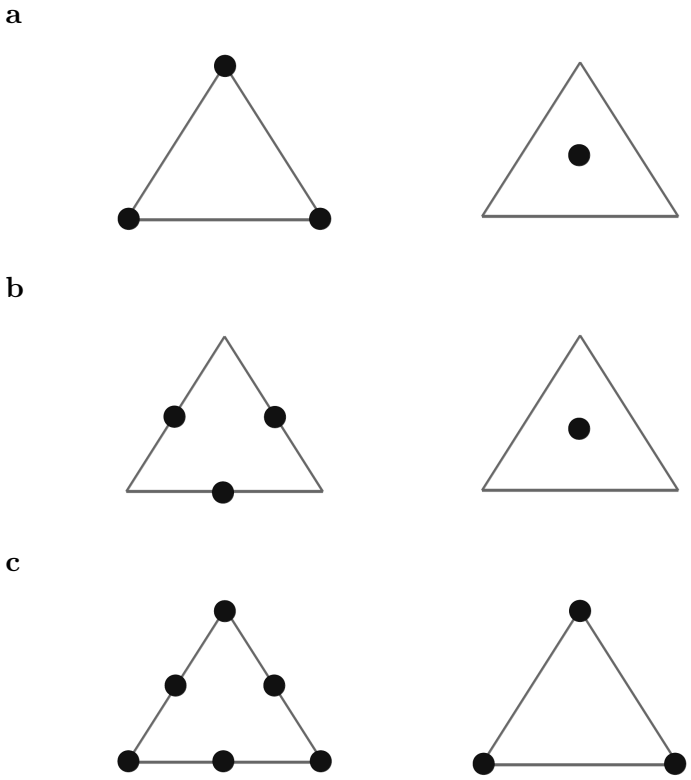

Figure 4: Proposed Finite Element Method for the primal problem (100). The couple $(p, \mathbf{u}) \in H^1(\Omega) \times L^2(\Omega)$ is approximated using (a) linear P_1 Lagrange elements $\left(\mathcal{C}_1^0(\Omega), \boldsymbol{\mathcal{C}}_0(\Omega)\right)$, (b) lowest-order nonconforming Crouzeix-Raviart elements $\left(\mathcal{CR}_1^0(\Omega), \boldsymbol{\mathcal{C}}_0(\Omega)\right)$, (c) quadratic P_2 Lagrange elements $\left(\mathcal{C}_2^0(\Omega), \boldsymbol{\mathcal{C}}_1(\Omega)\right)$.

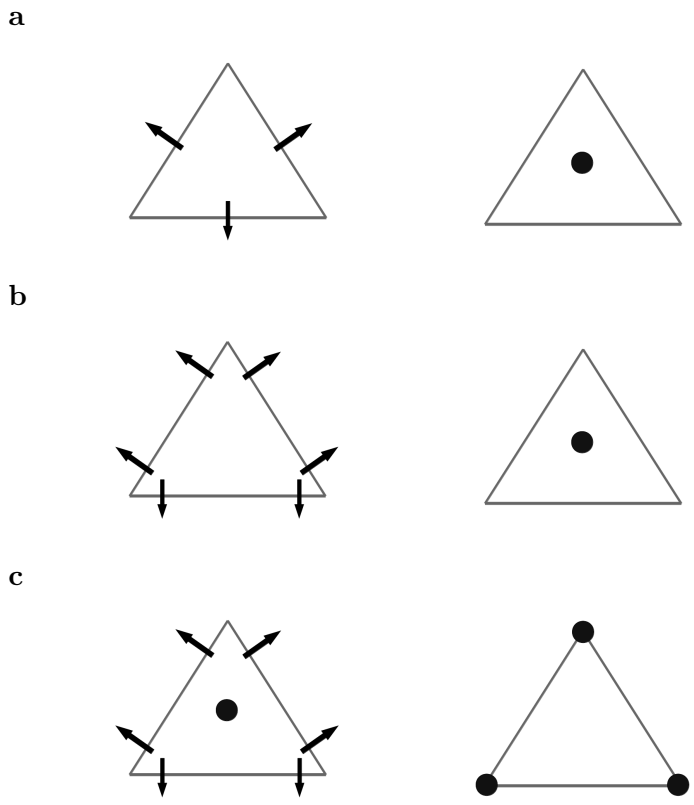

Figure 5: Proposed Finite Element Method for the mixed problem (99). The couple $(\mathbf{u}, p) \in \mathbf{H}(\mathrm{div}, \Omega) \times L^2(\Omega)$ is approximated using (a) lowest-order Raviart-Thomas elements $\left(\boldsymbol{\mathcal{RT}}_0(\Omega), \mathcal{C}_0^0(\Omega)\right)$, (b) lowest-order Brezzi-Douglas-Marini elements $\left(\boldsymbol{\mathcal{BDM}}_1(\Omega), \mathcal{C}_0^0(\Omega)\right)$, (c) first-order Raviart-Thomas elements $\left(\boldsymbol{\mathcal{RT}}_1(\Omega), \mathcal{C}_1^0(\Omega)\right)$.

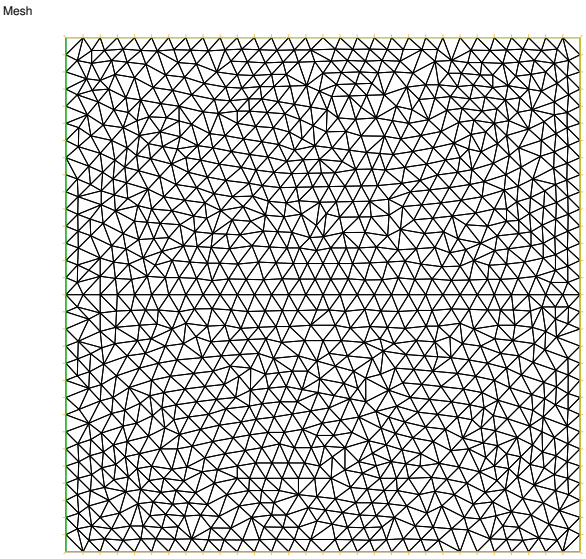

Figure 6: Computational mesh for the numerical simulations of Sec. 4.3. The biunit square $\Omega = [\,0,1\,]^2$ is discretized using $N = 30$ elements per face.

Concerning the primal Darcy's problem (100), we exploit the three proposed finite element methods to approximate the problem. A comparative 2D view of the three output is given in Figure 7. Figure 8 shows the numerical results of the linear Lagrange/Courant finite element method (83). In Figure 9 we report the approximated pressure and velocity from the lowest-order nonconforming Crouzeix-Raviart finite element method (87). Finally, Figure 10 shows the numerical solutions with quadratic Lagrange/Courant finite elements.

Similarly, for the mixed Darcy's problem (99), we test the three finite element methods proposed in Sec. 4.2. A comparative 2D view of the three couples of $\big($velocity, pressure$\big)$ solutions is given in Figure 11. Figure 12 shows the numerical results of the lowest-order Raviart-Thomas finite element method (90). In Figure **??** we report the approximated pressure and velocity from the lowest-order Brezzi-Douglas-Marini finite element method (91). Finally, Figure 14 shows the numerical solutions with first-order Raviart-Thomas finite elements.

4.4 Comparative error analysis

In the above section we discussed a *qualitative* comparison of numerical results from different finite element methods. Indeed, the aim of this section is to present a quantitative comparison of their accuracy. To this purpose, we will compute proper norms of the approximation errors, namely $\| p - p_h \|$ and $\| \mathbf{u} - \mathbf{u}_h \|$. We consider four computational mesh with characteristic size that halves at each step [see Fig. 15].

a

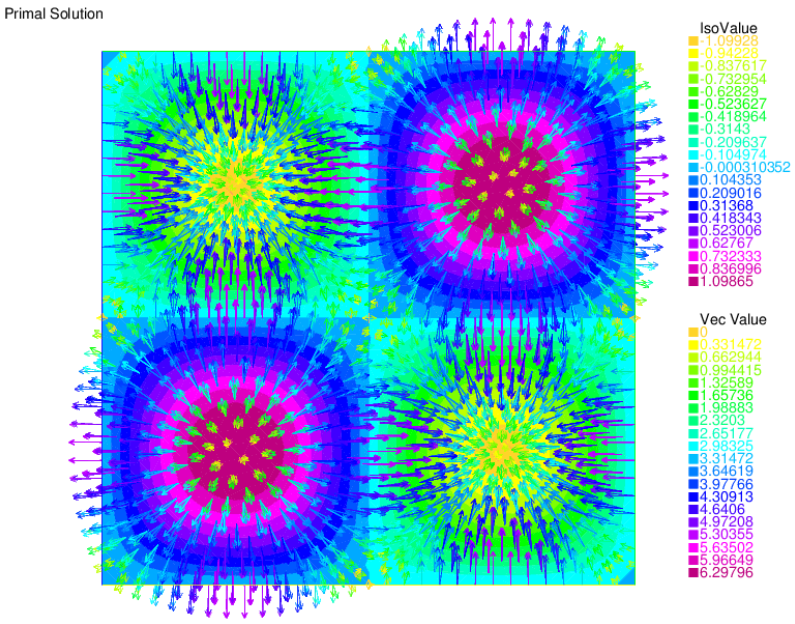
Primal Solution
IsoValue
-1.09528
-0.94228
-0.837617
-0.732954
-0.62829
-0.523627
-0.418964
-0.3143
-0.209637
-0.104974
-0.000310352
0.104353
0.209016
0.31368
0.418343
0.523006
0.62767
0.732333
0.836996
1.09865
Vec Value
0
0.331472
0.662944
0.994415
1.32589
1.65736
1.98883
2.3203
2.65177
2.98325
3.31472
3.64619
3.97766
4.30913
4.6406
4.97208
5.30355
5.63502
5.96649
6.29796

b

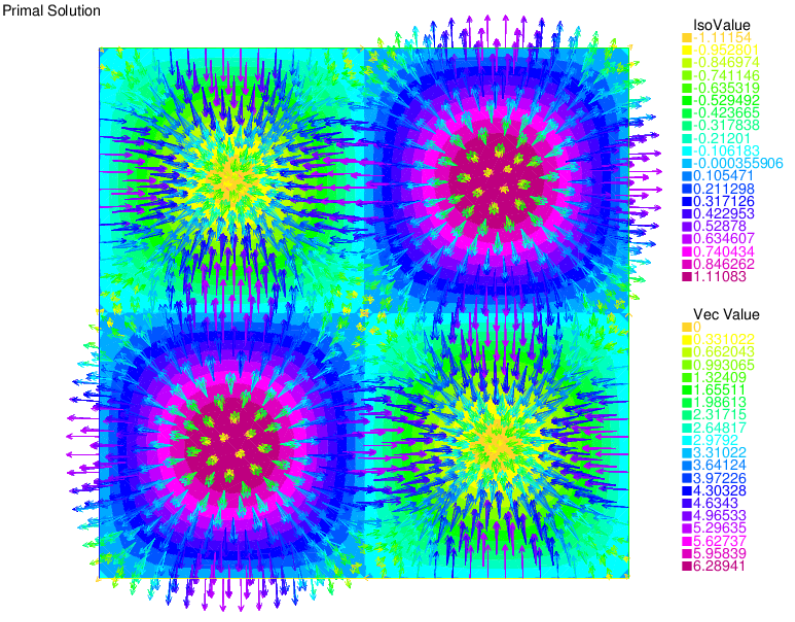
Primal Solution
IsoValue
-1.11154
-0.952801
-0.846974
-0.741146
-0.635319
-0.529492
-0.423665
-0.317838
-0.21201
-0.106183
-0.000355906
0.105471
0.211298
0.317126
0.422953
0.52878
0.634607
0.740434
0.846262
1.11083
Vec Value
0
0.331022
0.662043
0.993065
1.32409
1.65511
1.98613
2.31715
2.64817
2.9792
3.31022
3.64124
3.97226
4.30328
4.6343
4.96533
5.29635
5.62737
5.95839
6.28941

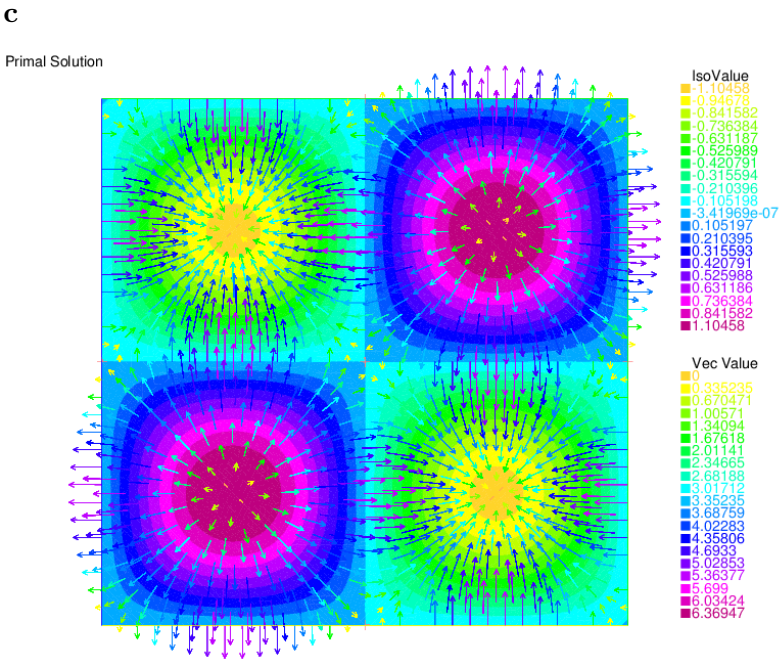

Figure 7: Numerical solutions of the primal problem (100). A coupled "D pressure-velocity plot is reported. From the top to the bottom panel we have: (a) $(p_h, \mathbf{u}_h) \in \mathcal{C}_1^0(\Omega) \times \boldsymbol{\mathcal{C}}_0(\Omega)$, (b) $(p_h, \mathbf{u}_h) \in \mathcal{CR}_1^0(\Omega) \times \boldsymbol{\mathcal{C}}_0(\Omega)$, (c) $(p_h, \mathbf{u}_h) \in \mathcal{C}_2^0(\Omega) \times \boldsymbol{\mathcal{C}}_1(\Omega)$.

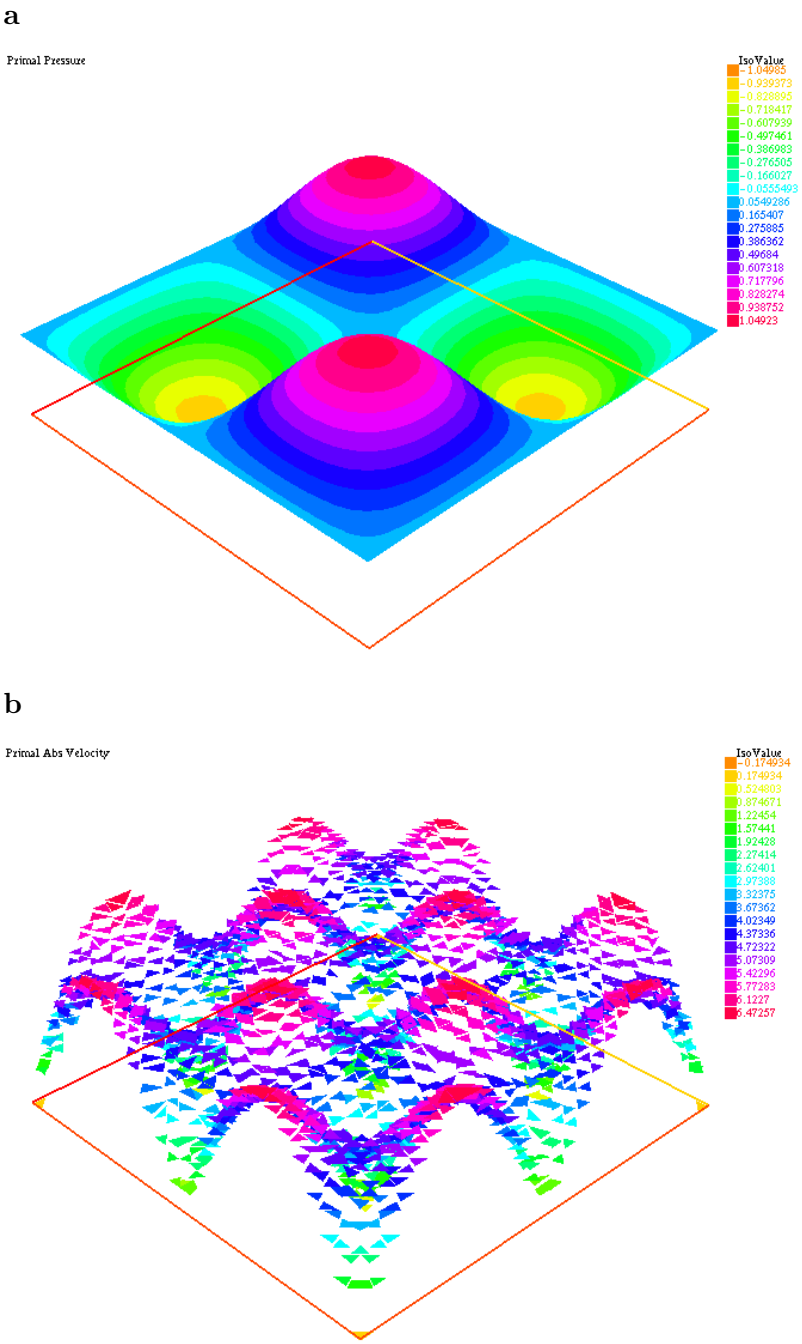

Figure 8: Numerical solutions $(p_h, \mathbf{u}_h) \in \mathcal{C}_1^0(\Omega) \times \boldsymbol{\mathcal{C}}_0(\Omega)$ of the primal finite element model (83) for $k = 1$. (a) On the left the approximated pressure field, (b) on the right the approximated velocity magnitude.

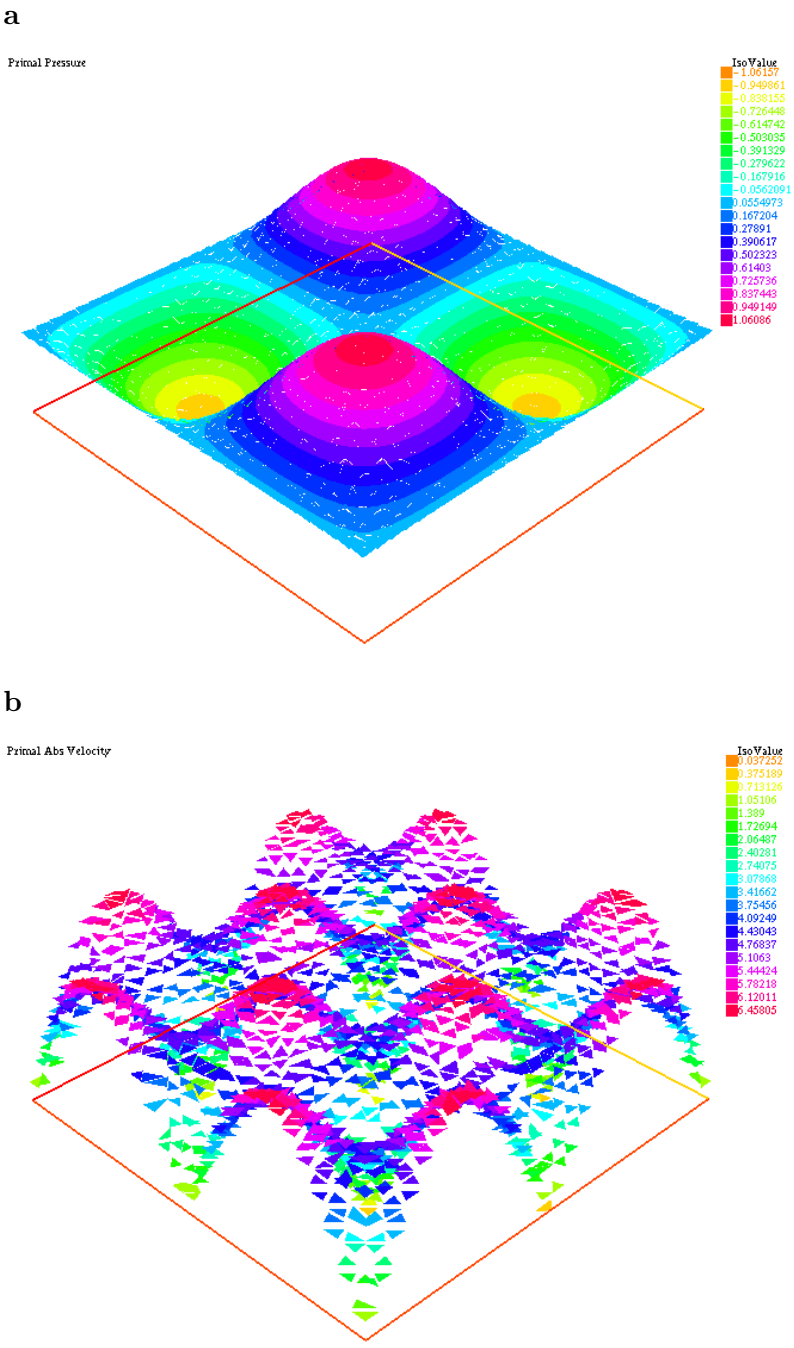

Figure 9: Numerical solutions $(p_h, \mathbf{u}_h) \in \mathcal{CR}_1^0(\Omega) \times \boldsymbol{\mathcal{C}}_0(\Omega)$ of the primal finite element model (87) for $k = 1$. (a) On the left the approximated pressure field, (b) on the right the approximated velocity magnitude.

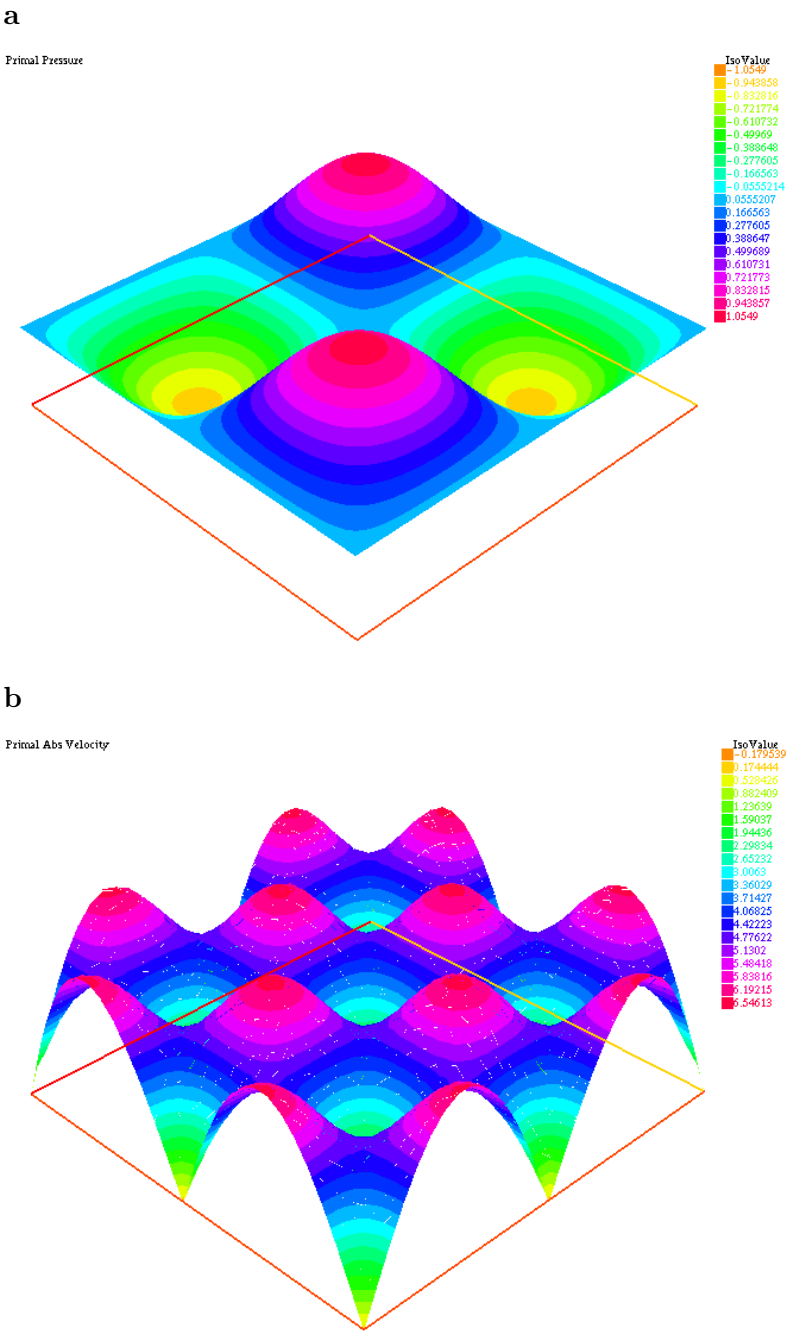

Figure 10: Numerical solutions $(p_h, \mathbf{u}_h) \in \mathcal{C}_2^0(\Omega) \times \boldsymbol{\mathcal{C}}_1(\Omega)$ of the primal finite element model (83) for $k = 2$. (a) On the left the approximated pressure field, (b) on the right the approximated velocity magnitude.

a

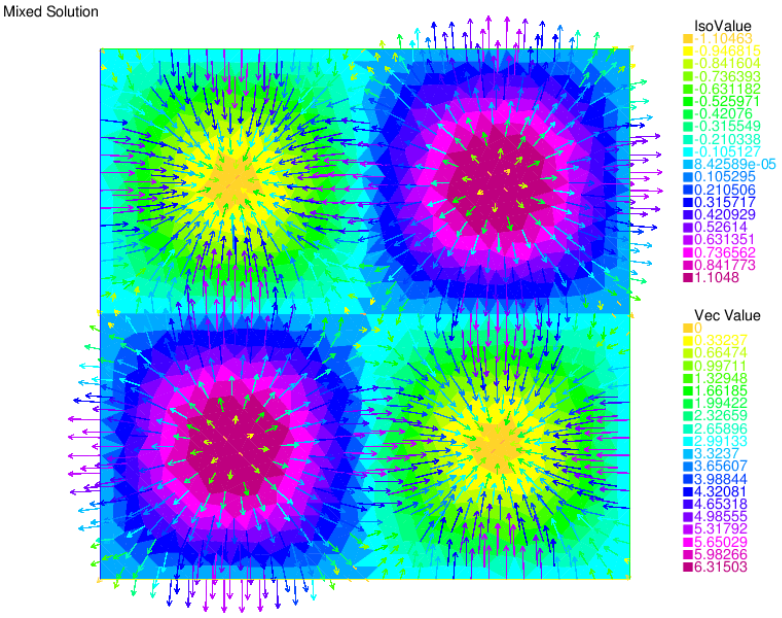
Mixed Solution
IsoValue
-1.10463
-0.946815
-0.841604
-0.736393
-0.631182
-0.525971
-0.42076
-0.315549
-0.210338
-0.105127
8.42589e-05
0.105295
0.210506
0.315717
0.420929
0.52614
0.631351
0.736562
0.841773
1.1048
Vec Value
0
0.33237
0.66474
0.99711
1.32948
1.66185
1.99422
2.32659
2.65896
2.99133
3.3237
3.65607
3.98844
4.32081
4.65318
4.98555
5.31792
5.65029
5.98266
6.31503

b

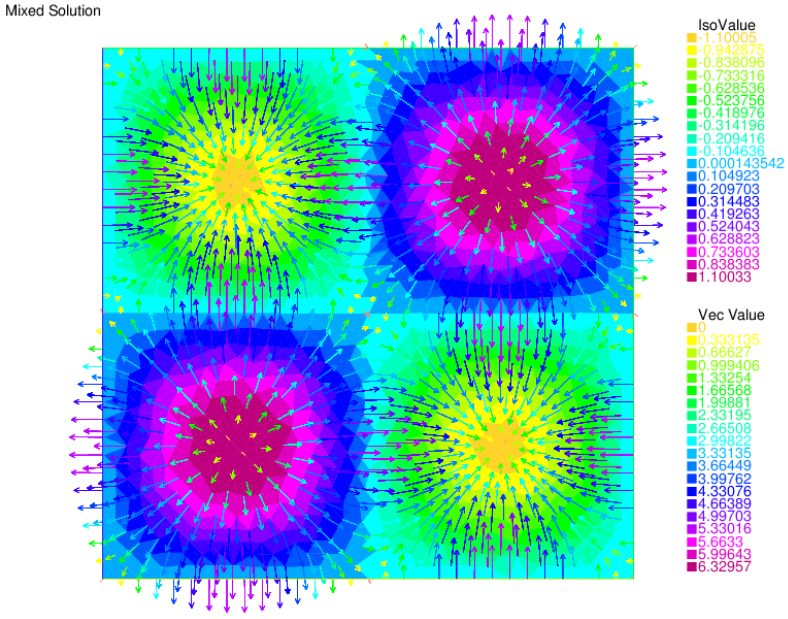
Mixed Solution
IsoValue
-1.10005
-0.942575
-0.838096
-0.733616
-0.628536
-0.523756
-0.418976
-0.314196
-0.209416
-0.104636
0.000143542
0.104923
0.209703
0.314483
0.419263
0.524043
0.628823
0.733603
0.838383
1.10033
Vec Value
0
0.333135
0.66627
0.999406
1.33254
1.66568
1.99881
2.33195
2.66508
2.99822
3.33135
3.66449
3.99762
4.33076
4.66389
4.99703
5.33016
5.6633
5.99643
6.32957

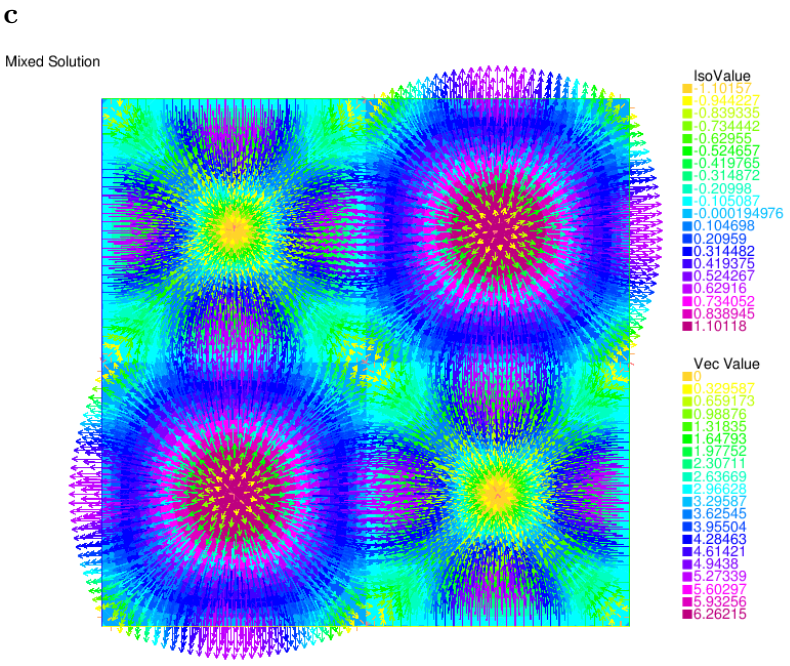

Figure 11: Numerical solutions of the mixed problem (99). A coupled 2D pressure-velocity plot is reported. From the top to the bottom panel we have: (a) $(\mathbf{u}_h, p_h) \in \boldsymbol{\mathcal{RT}}_0(\Omega) \times \mathcal{C}_0^0(\Omega)$, (b) $(\mathbf{u}_h, p_h) \in \boldsymbol{\mathcal{BDM}}_1(\Omega) \times \mathcal{C}_0^0(\Omega)$, (c) $(\mathbf{u}_h, p_h) \in \boldsymbol{\mathcal{RT}}_1(\Omega) \times \mathcal{C}_1^0(\Omega)$.

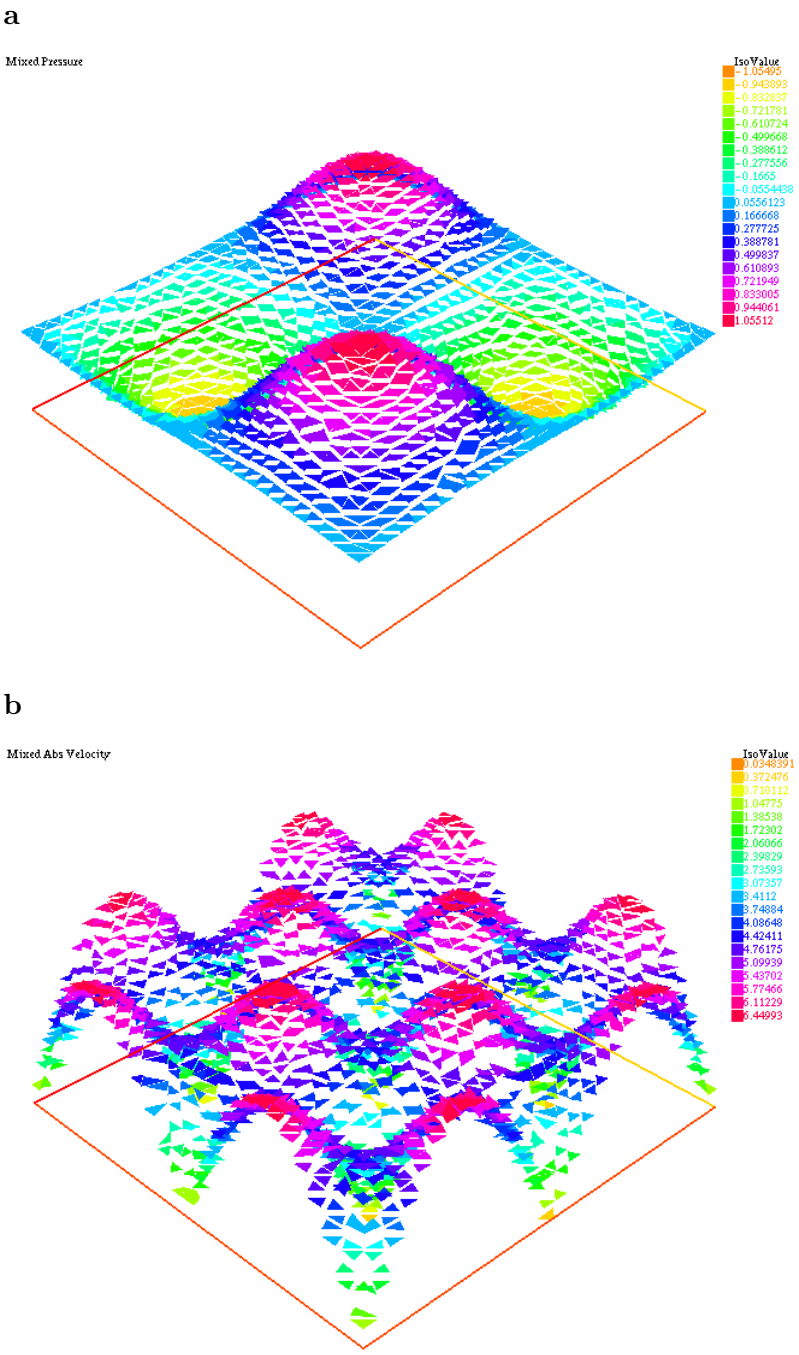

Figure 12: Numerical solutions $(\mathbf{u}_h, p_h) \in \boldsymbol{\mathcal{RT}}_0(\Omega) \times \mathcal{C}_0^0(\Omega)$ of the mixed finite element model (90) for $k = 0$. (a) On the left the approximated pressure field, (b) on the right the approximated velocity magnitude.

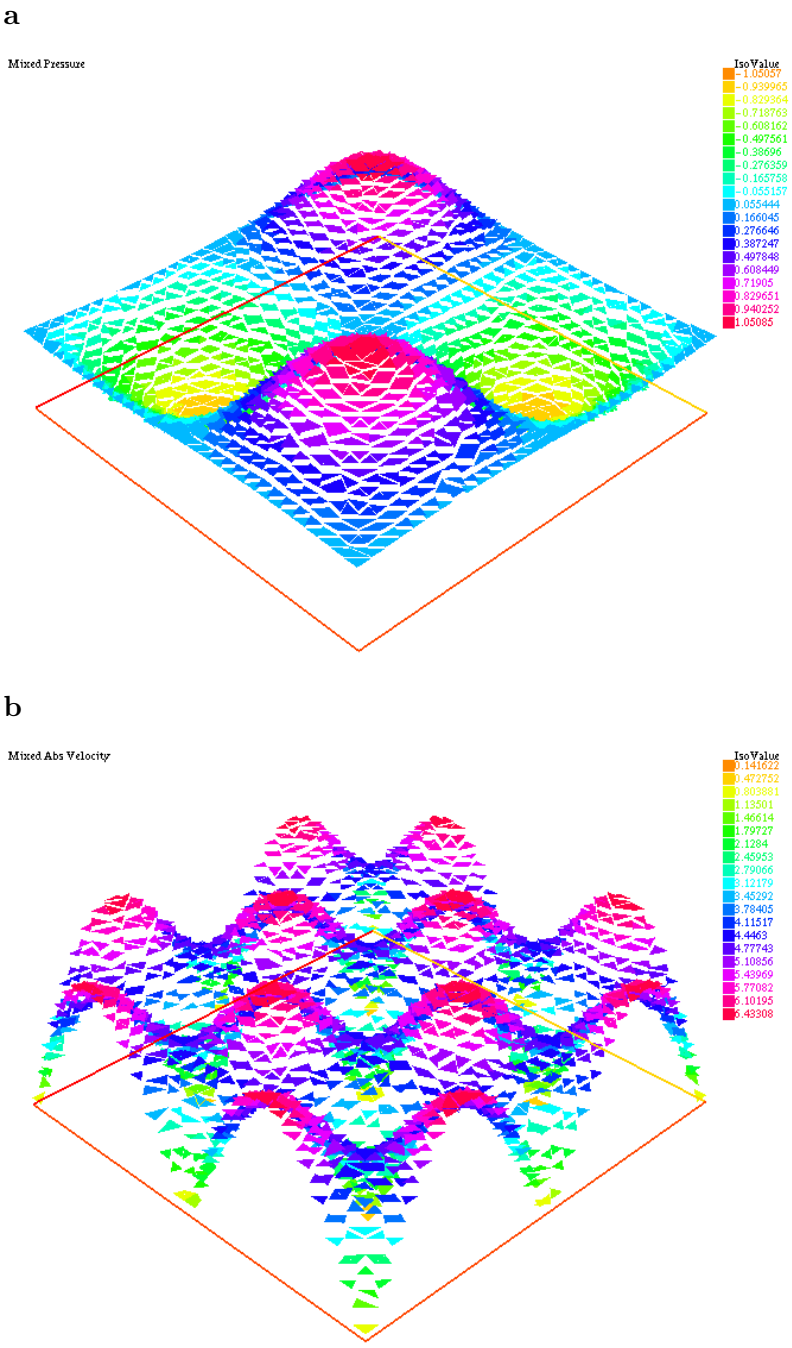

Figure 13: Numerical solutions $(\mathbf{u}_h, p_h) \in \boldsymbol{\mathcal{BDM}}_1(\Omega) \times \mathcal{C}_0^0(\Omega)$ of the mixed finite element model (91) for $k = 1$. (a) On the left the approximated pressure field, (b) on the right the approximated velocity magnitude.

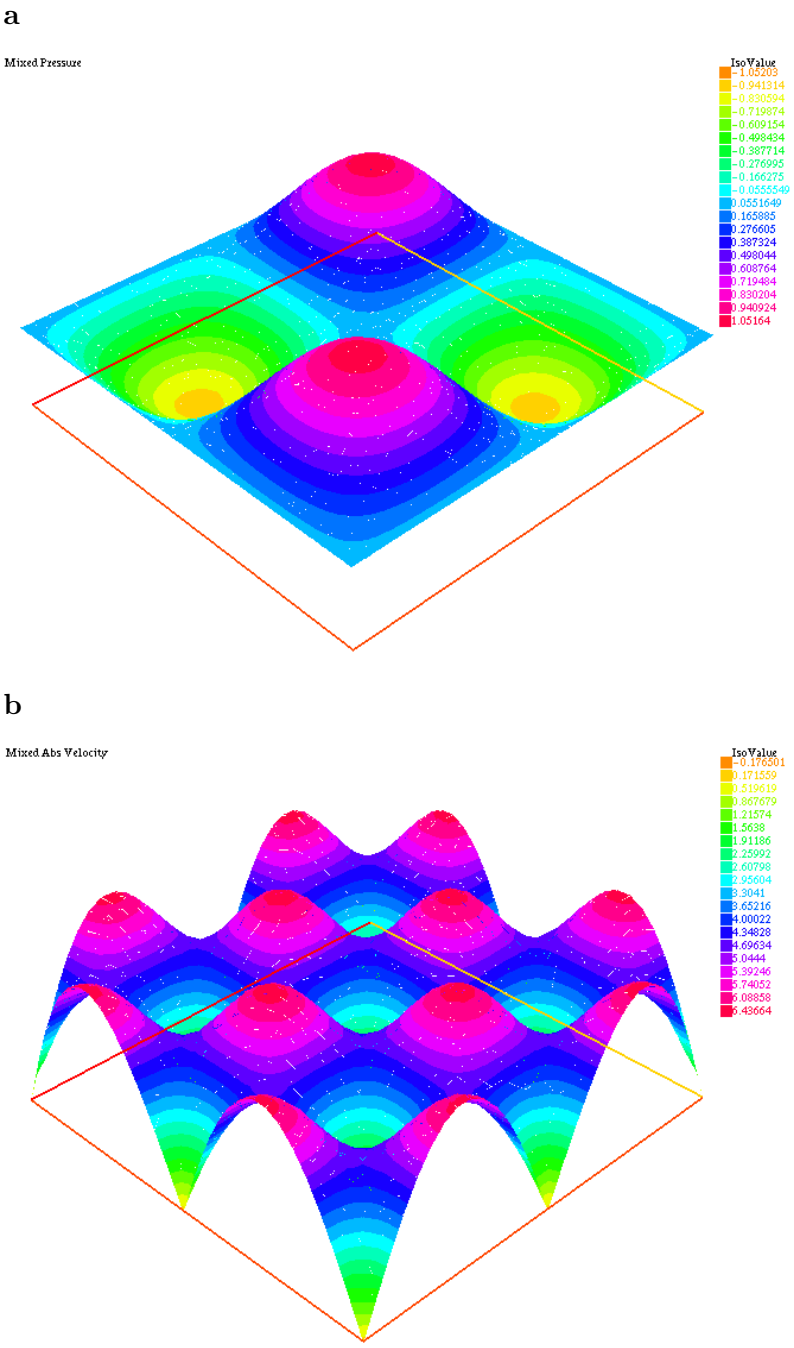

Figure 14: Numerical solutions $(\mathbf{u}_h, p_h) \in \boldsymbol{\mathcal{RT}}_1(\Omega) \times \mathcal{C}_1^0(\Omega)$ of the mixed finite element model (90) for $k = 1$. (a) On the left the approximated pressure field, (b) on the right the approximated velocity magnitude.

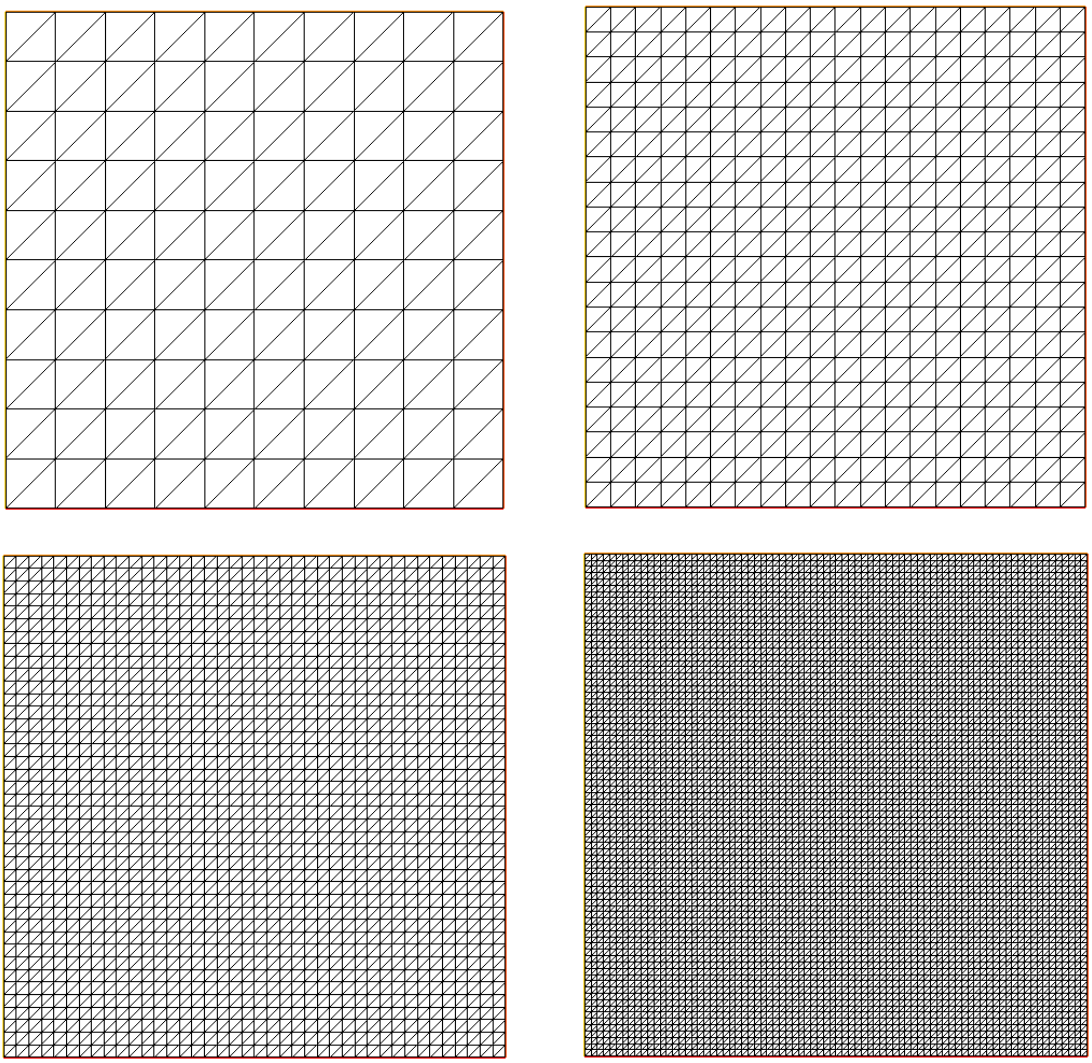

Figure 15: Computational meshes for the error analysis of Sec. 4.4. Moving from the top-left to the bottom-righ panel we have $h = 1/10$, $h = 1/20$, $h = 1/40$, $h = 1/80$

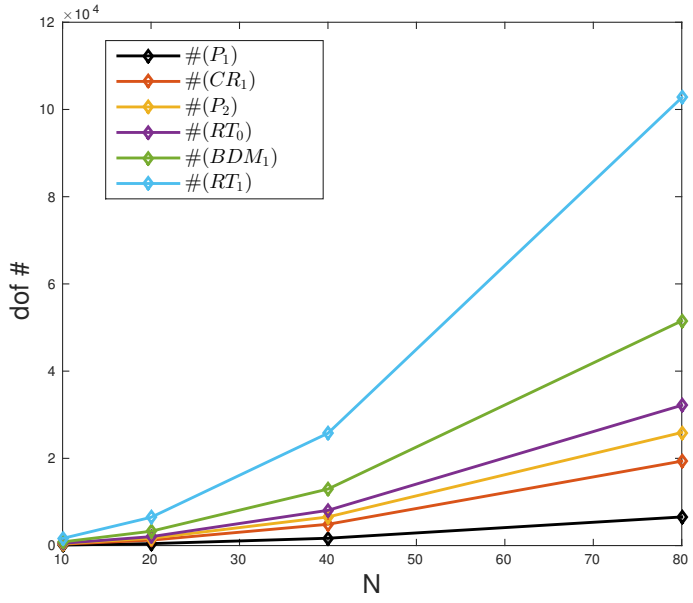

Figure 16: Number of degrees of freedom of provided primal and mixed FEM.

First, to give an idea of the FEM's computational cost we plot the number of degrees of freedom (dof) of each scheme in correspondence of the four proposed settings, i.e. for $N = 1/h = 10, 20, 40, 80$ elements per edge. Figure 16 confirms the expected relation, namely $\#dof(P_1) < \#dof(\mathcal{CR}_1) < \#dof(P_2) < \#dof(\mathcal{RT}_0) < \#dof(\mathcal{BDM}_1) < \#dof(\mathcal{RT}_1)$.

Let us now discuss the convergence for the primal problem (100). In Fig. 17 we report both the L^2 and H^1 norms of the pressure error, while for the velocity approximation we obviously consider only the L^2 norm. As expected from the Convergence Analysis of the Taylor-Hood finite elements (P_{k+1}, P_k) for the Poisson's problem [21], we have that the H^m-norm of the pressure's error scales as h^{k+1-m} for $k = 1, 2$ and $m = 0, 1$. Moreover, the L^2 norm of the velocity's error scales as h^{k-m}.

For the approximation of the mixed problem (99), we report the L^2 and $H(div)$ norms of the velocity error, while for the approximation of the pressure field we only consider the L^2 norm. Figures 18 confirms the results from the Theory of Mixed Finite Element Methods [cfr. Section 1]. Specifically, the natural $H(div)$ norms of the RT-MFEM error scales as h^{k+1}, while we loss an order of accuracy with BDM-MFEM. Nevertheless, the latter shows a better asymptotic behaviour than the former if we consider only the L^2-norm of the velocity's error (we have quadratic convergence for $k = 1$). Coherently, the L^2-norm of the pressure error scales linearly with k.

The above numerical results of the accuracy analysis of the six families of finite element

a

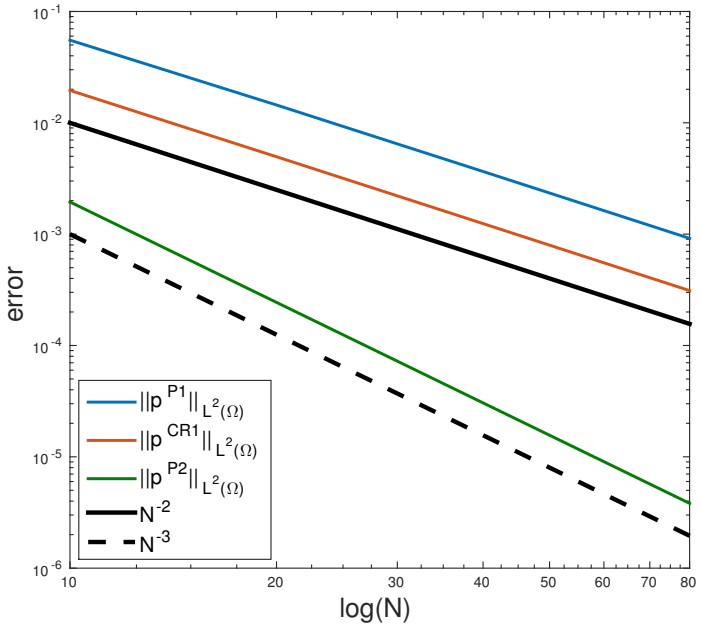
error
log(N)
$||p^{P1}||_{L^2(\Omega)}$
$||p^{CR1}||_{L^2(\Omega)}$
$||p^{P2}||_{L^2(\Omega)}$
N^{-2}
N^{-3}

b

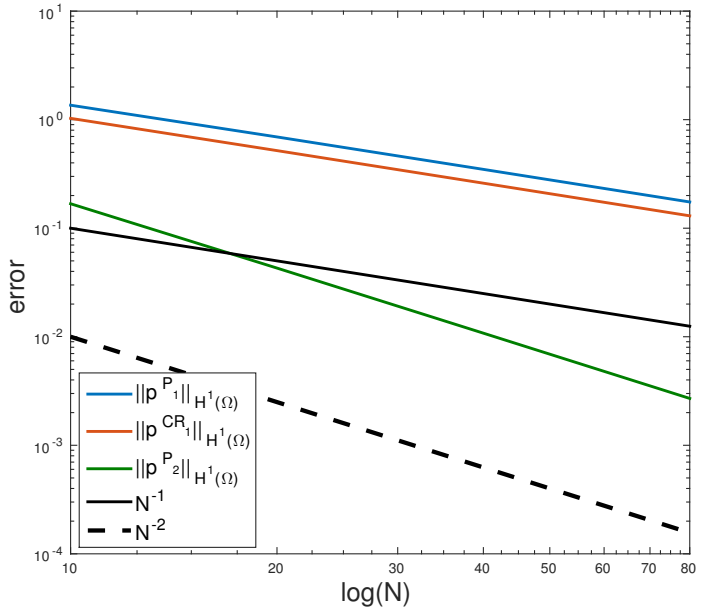
error
log(N)
$||p^{P_1}||_{H^1(\Omega)}$
$||p^{CR_1}||_{H^1(\Omega)}$
$||p^{P_2}||_{H^1(\Omega)}$
N^{-1}
N^{-2}

c

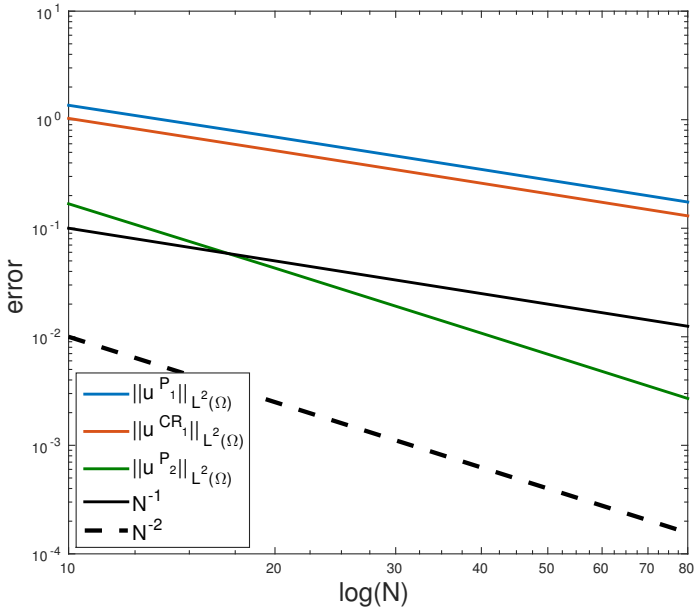

Figure 17: Convergence analysis for the approximation of the primal problem (100). We plot the error norms in logarithmic scale for $N = 1/h = 10, 20, 40, 80$. (a) $\| p - p_h \|_{L^2(\Omega)}$, (b) $\| p - p_h \|_{H^1(\Omega)}$, (c) $\| \mathbf{u} - \mathbf{u}_h \|_{L^2(\Omega)}$.

a

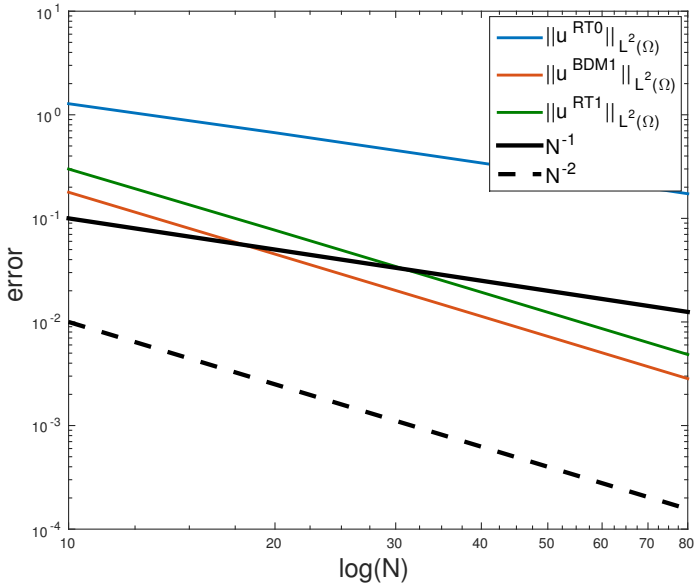
$||u^{RT0}||_{L^2(\Omega)}$
$||u^{BDM1}||_{L^2(\Omega)}$
$||u^{RT1}||_{L^2(\Omega)}$
N^{-1}
N^{-2}
error
log(N)

b

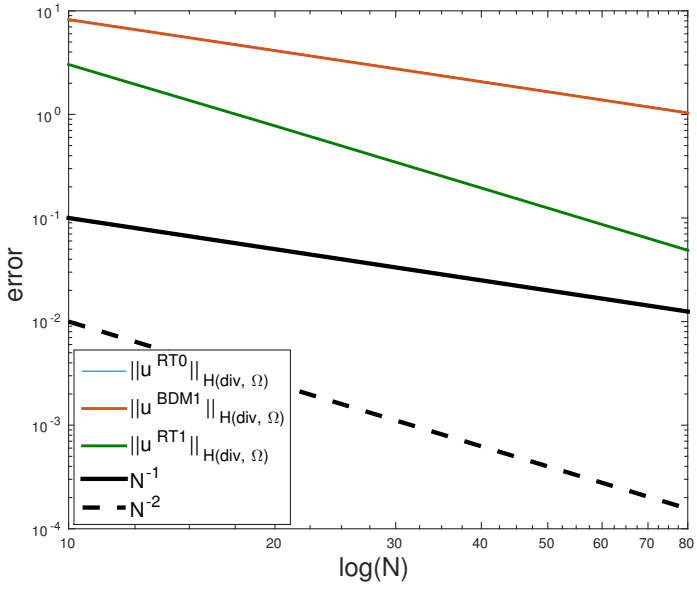
$||u^{RT0}||_{H(div,\ \Omega)}$
$||u^{BDM1}||_{H(div,\ \Omega)}$
$||u^{RT1}||_{H(div,\ \Omega)}$
N^{-1}
N^{-2}
error
log(N)

c

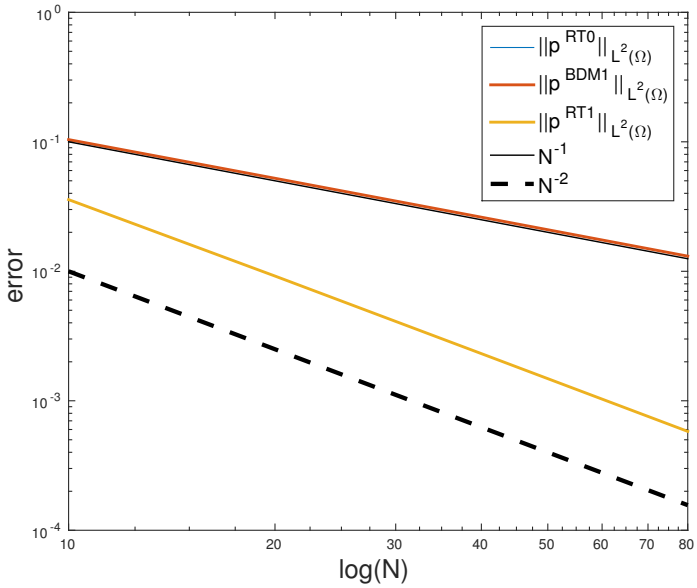

Figure 18: Convergence analysis for the approximation of the mixed problem (99). We plot the error norms in logarithmic scale for $N = 1/h = 10, 20, 40, 80$. (a) $\| \mathbf{u} - \mathbf{u}_h \|_{L^2(\Omega)}$, (b) $\| \mathbf{u} - \mathbf{u}_h \|_{\mathbf{H}(\mathrm{div},\Omega)}$, (c) $\| p - p_h \|_{L^2(\Omega)}$.

methods are summarized in the following table:

FEM	$err_h(p,0)$	$err_h(p,1)$	$err_h(\mathbf{u},0)$	$err_h(\mathbf{u},\mathrm{div})$
$\mathcal{C}_1$	$\mathcal{O}(h^2)$	$\mathcal{O}(h^1)$	$\mathcal{O}(h^1)$	—
$\mathcal{CR}_1$	$\mathcal{O}(h^2)$	$\mathcal{O}(h^1)$	$\mathcal{O}(h^1)$	—
$\mathcal{C}_2$	$\mathcal{O}(h^3)$	$\mathcal{O}(h^2)$	$\mathcal{O}(h^2)$	—
$\mathcal{RT}_0$	$\mathcal{O}(h^1)$	—	$\mathcal{O}(h^1)$	$\mathcal{O}(h^1)$
$\mathcal{BDM}_1$	$\mathcal{O}(h^1)$	—	$\mathcal{O}(h^2)$	$\mathcal{O}(h^1)$
$\mathcal{RT}_1$	$\mathcal{O}(h^2)$	—	$\mathcal{O}(h^2)$	$\mathcal{O}(h^2)$

where we adopted, for simplicity, the notation $err_h(p,m) := \| p - p_h \|_{H^m(\Omega)}$. In conclusion, our finite element solver complies with theoretical results.

A Code documentation

The last stable release of the code is available at

`https://github.com/domeniconotaro/NAPDE`

The package is organized as follows:

- `assembling.edp` : definition of the primal and mixed variational problems
- `fem.edp` : list of available finite element methods
- `macros.edp` : definition of useful macros
- `main.edp` : main program to compare the primal and mixed solutions
- `mesh.edp` : generatation of the computational mesh
- `README` : instructions to run the program

In the remainder we give a brief guide for the code.

`mesh.edp`

The initial step is to build a proper computational mesh $\mathcal{T}_h$. In the example of Sec. 4.1 we propose a squared mesh with variable number of subdivisions per edge. Please choose the desired mesh size as $h = 1/N_{subdiv}$.

```
// ********************************************************************
//  FILE        : mesh.edp
//  DESCRIPTION : generatation of the computational mesh
//  AUTHOR      : D. Notaro <domenico.not@gmail.com>
// ********************************************************************
//
//  Aux variables
// ______________________________________
string savedir = "./results/";         // output directory
string prefix  = "darcy_N=10_";        // problem prefix used in output
bool REGULAR = false;                  // regular/not triangulation
//
//  Boundary definition
// ______________________________________
border l0(t=0,1) { x = t ;  y = 0;   label = 1;}
border l1(t=0,1) { x = 1;   y = t;   label = 2;}
border l2(t=0,1) { x = 1-t; y = 1;   label = 2;}
border l3(t=0,1) { x = 0;   y = 1-t; label = 4;}
//
```

```
//  Geometry definition
// _____________________________________
int nbdiv = 10;
func geom = l0(nbdiv)+l1(nbdiv)+l2(nbdiv)+l3(nbdiv);
plot(geom,wait=1,ps=savedir+prefix+"geom.eps",cmm="geom");
//
//  Mesh generation
// _____________________________________
mesh Th;
if (REGULAR)
        Th = square(nbdiv,nbdiv);
else
        Th = buildmesh(geom);
//
//  Visualization
// _____________________________________
plot(Th,wait=1,ps=savedir+prefix+"mesh.eps",cmm="Mesh");
```

fem.edp

As a first significant step, the user has to select the desired finite element approximation for both the primal and mixed problems. Specifically, one has to uncomment a specific (pressure, velocity) pair of FE space for the primal problem and/or a (velocity, pressure) pair of FE space for the primal problem. In the following example, we select linear Lagrange elements for the primal pressure and the lowest-order Raviart-Thomas elements for the mixed velocity.

```
// ********************************************************************
//  FILE        : fem.edp
//  DESCRIPTION : list of available finite element methods
//  AUTHOR      : D. Notaro <domenico.not@gmail.com>
// ********************************************************************
//
//  Header files
// ____________________________________________
load "Element_Mixte"                    // implementation of BDM1, RT1
include "mesh.edp"                      // domain triangulation
//
//  Primal FE spaces and functions
// ____________________________________________
/* Conforming linear Courant (P1) */
fespace Vh(Th,P1), VVh(Th,[P0,P0]);
/* Non-conforming Crouzeix-Raviart (CR) */
//fespace Vh(Th,P1nc), VVh(Th,[P0,P0]);
```

```
/* Conforming quadratic Courant (P2) */
//fespace Vh(Th,P2), VVh(Th,[P1dc,P1dc]);
/* Pressure trial and test functions */
Vh pp,qp;
/* Velocity trial functions */
VVh [up1,up2];
/* Primal dimensions */
real dimVh = Vh.ndof;
real dimVVh = VVh.ndof;
//
//   Mixed FE spaces and functions
// _____________________________________
/* Lowest-order Raviart-Thomas (RT0) */
fespace Wh(Th,RT0),Qh(Th,P0),Ih(Th,[P1,P1]);
/* Lowest-order Brezzi-Douglas-Marini (BDM1) */
//fespace Wh(Th,BDM1),Qh(Th,P0),Ih(Th,BDM1);
/* First-order  Raviart-Thomas (RT1) */
//fespace Wh(Th,RT1),Qh(Th,P1dc),Ih(Th,RT1);
/* Velocity trial and test functions */
Wh [u1,u2],[v1,v2];
/* Pressure trial and test functions */
Qh p,q;
/* Mixed dimensions */
real dimWh = Wh.ndof;
real dimQh = Qh.ndof;
real dimTot = dimWh+dimQh;
```

assembling.edp

If needed, the user can *modify* the problem, e.g. the permeability of the medium or the boundary data, by editing the following file.

```
// ********************************************************************
//  FILE        : assembling.edp
//  DESCRIPTION : primal and mixed variational problems
//  AUTHOR      : D. Notaro <domenico.not@gmail.com>
// ********************************************************************
//
//  Header files
// _____________________________________
include "fem.edp"                       // FE spaces and functions
//
//  Aux variables
// _____________________________________
real TOL     = 1.e-08;                  // max tolerance
```

```
bool PRECOND = false;                    // do/do not precond
//
//  Data
// ____________________________________________
/* Medium permeability */
real kappa = 1.;
/* Divergence source */
func f = 8*pi*pi*kappa*sin(2*pi*x)*sin(2*pi*y);
Qh fh = f;
/* Boundary data */
func g = 0.;
/* Exact pressure */
func pe   = sin(2*pi*x)*sin(2*pi*y);
func pedx = 2*pi*cos(2*pi*x)*sin(2*pi*y);
func pedy = 2*pi*sin(2*pi*x)*cos(2*pi*y);
/* Exact velocity */
func ue1 = -2*pi*kappa*cos(2*pi*x)*sin(2*pi*y);
func ue2 = -2*pi*kappa*sin(2*pi*x)*cos(2*pi*y);
func ue1dx = 4*pi*pi*kappa*sin(2*pi*x)*sin(2*pi*y);
func ue2dy = 4*pi*pi*kappa*sin(2*pi*x)*sin(2*pi*y);
//
//  Primal problem definition
// ____________________________________________
problem primalDarcy(pp,qp,solver=CG,eps=-TOL) =
     int2d(Th) ( dx(pp)*dx(qp) + dy(pp)*dy(qp) )
        - int2d(Th) ( f*qp )
        + on ( 1,2,3,4, pp=g );
//
//  Mixed problem definition
// ____________________________________________
/* Variational forms */
varf a([u1,u2],[v1,v2]) =
        int2d(Th) ( 1./kappa*u1*v1 + 1./kappa*u2*v2 );
varf b([u1,u2],[q]) =
        int2d(Th) ( (dx(u1) + dy(u2))*q ) ;
varf bt([p],[v1,v2]) =
        int2d(Th) ( -p*(dx(v1) + dy(v2)) ) ;
varf rhs(p,q) =
        int2d(Th) ( fh*q );
/* Matrices */
matrix A = a(Wh,Wh);
matrix B = b(Wh,Qh);
matrix Bt = bt(Qh,Wh);
matrix AM = [[A,Bt],[B,0]];
set(AM,solver=GMRES);
real[int] FM(dimTot);
```

```
FM(dimWh:dimTot-1) = rhs(0,Qh);
real[int] UM(dimTot);
/* Block preconditioner */
matrix PM;
if (PRECOND) {
varf masspres(p,q) = int2d(Th) ( p*q );
matrix MP = masspres(Qh,Qh);
PM = [[A,0],[0,MP]];
set(PM,solver=UMFPACK);
}
else {
real[int] one(dimTot); one = 1.;
PM = one;
set(PM,solver=UMFPACK);
}
/* Residual computation */
real[int] R(dimTot);
func real[int] BlockDiag(real[int] &xx){
  verbosity=1;
  R=PM^-1*xx;
  verbosity=3;
  return R;
}
int i=0;
func real[int] MatVec(real[int] &xx){
  R=AM*xx;
  i++;
  if (i%50==0) cout<<"GMRES: iter "<< i <<endl;
  return R;
}
```

main.edp

Finally, the user can run the program to build and solve both the primal and mixed problems. Numerical results are first compared from a qualitative point of view (plot of computed and expected solutions). Finally an error analysis is performed to quantify the goodness of provided FEMs.

```
// ********************************************************************
//  FILE        : main.edp
//  DESCRIPTION : program to compare the primal and mixed solutions
//  AUTHOR      : D. Notaro <domenico.not@gmail.com>
// ********************************************************************
//
```

```
//  Header files
// ________________________________________
include "macros.edp"                        // definition of Grad, Div,...
include "assembling.edp"                    // primal and mixed problems
//
//  Output flags
// ________________________________________
bool PLOT   = false;                        // do/do not plot solutions
bool EXACT  = false;                        // do/do not plot ex solutions
bool EXPORT = false;                        // do/do not export solutions
bool ERROR  = true;                         // do/do not compute the
   errors
//
//  Primal solution
// ________________________________________
/* Compute pressure and velocity */
real start = clock();
primalDarcy;
real cpup = clock()-start;
[up1,up2] = [-kappa*dx(pp),-kappa*dy(pp)];
/* Export results */
if (EXPORT) {
ofstream solp("primal_solution");
solp << "up1 : " << up1[] << endl
           << "up2 : " << up2[] << endl
           << "pp  : " << pp[]  << endl;
}
/* Compute velocity div and magnitude */
Qh divup = Div(up1,up2);
Qh ump   = Magnitude(up1,up2);
//
//  Mixed solution
// ________________________________________
/* Compute pressure and velocity */
start = clock();
//mixedDarcy;
LinearGMRES(MatVec, UM, FM, nbiter=10000, eps=TOL, precon=BlockDiag);
real cpum = clock()-start;
verbosity = 2;
u1[] = UM(0:dimWh-1);
p[]  = UM(dimWh:dimTot-1);
/* Export results */
if (EXPORT) {
ofstream solm("mixed_solution");
solm << UM << endl;
}
```

```
/* Interpole on Pk for postprocessing (needed for RT0) */
Ih [u1int, u2int] = [u1,u2];
/* Compute velocity div and magnitude */
Qh divu = Div(u1,u2);
Qh um   = Magnitude(u1,u2);
//
//  Solving report
// ____________________________________
cout << "==============================" << endl;
cout << " primal dof : " << dimVh         << endl;
cout << " primal CPU : " << cpup << "s"   << endl;
cout << " mixed  dof : " << dimTot        << endl;
cout << " mixed  CPU : " << cpum << "s"   << endl;
cout << "==============================" << endl;
//
//  Visual comparison
// ____________________________________
/*  Zoom box [(xmin,ymin),(xmax,ymax)] */
func zoom2d = [
    [ -0.1, -0.2 ],
    [  1.2,  1.1 ] ];
func zoom3d = [
    [ 0.1, 0.2 ],
    [ 0.9, 1.0 ] ];
//* Exact */
if (EXACT) {
fespace Ph(Th, P2);
Ph peh = pe;
Ph ue1h = ue1, ue2h = ue2;
Ph umeh = Magnitude(ue1, ue2);
Ph ffh = f;
plot (peh, wait=1,value=1,fill=1,dim=3,bb=zoom3d,
        ps=savedir+prefix+"pe.png",cmm="Exact Pressure");
plot (ue1h,wait=1,value=1,fill=1,dim=3,bb=zoom3d,
        ps=savedir+prefix+"u1e.png",cmm="Exact X Velocity");
plot (ue2h,wait=1,value=1,fill=1,dim=3,bb=zoom3d,
        ps=savedir+prefix+"u2e.png",cmm="Exact Y Velocity");
plot (umeh,wait=1,value=1,fill=1,dim=3,bb=zoom3d,
        ps=savedir+prefix+"ume.png",cmm="Exact Abs Velocity");
plot (ffh,wait=1,value=1,fill=1,dim=3,bb=zoom3d,
        ps=savedir+prefix+"f.png",cmm="Exact Div Velocity");
}
if (PLOT) {
/* Primal */
plot (pp,[up1,up2],wait=1,value=1,fill=1,dim=2,coef=0.01,bb=zoom2d,
        ps=savedir+prefix+"primal.png",cmm="Primal Solution");
```

```
plot (pp, wait=1,value=1,fill=1,dim=3,bb=zoom3d,
        ps=savedir+prefix+"pp.png",cmm="Primal Pressure");
plot (up1,wait=1,value=1,fill=1,dim=3,bb=zoom3d,
        ps=savedir+prefix+"u1p.png",cmm="Primal X Velocity");
plot (up2,wait=1,value=1,fill=1,dim=3,bb=zoom3d,
        ps=savedir+prefix+"u2p.png",cmm="Primal Y Velocity");
plot (ump,wait=1,value=1,fill=1,dim=3,bb=zoom3d,
        ps=savedir+prefix+"ump.png",cmm="Primal Abs Velocity");
plot (divup,wait=1,value=1,fill=1,dim=3,bb=zoom3d,
        ps=savedir+prefix+"divup.png",cmm="Primal Velocity Div");
/* Mixed */
plot (p,[u1int,u2int],wait=1,value=1,fill=1,dim=2,coef=0.01,bb=zoom2d,
        ps=savedir+prefix+"mixed.png",cmm="Mixed Solution");
plot (p, wait=1,value=1,fill=1,dim=3,bb=zoom3d,
        ps=savedir+prefix+"p.png",cmm="Mixed Pressure");
plot (u1int,wait=1,value=1,fill=1,dim=3,bb=zoom3d,
        ps=savedir+prefix+"u1.png",cmm="Mixed X Velocity");
plot (u2int,wait=1,value=1,fill=1,dim=3,bb=zoom3d,
        ps=savedir+prefix+"u2.png",cmm="Mixed Y Velocity");
plot (um,wait=1,value=1,fill=1,dim=3,bb=zoom3d,
        ps=savedir+prefix+"um.png",cmm="Mixed Abs Velocity");
plot (divu,wait=1,value=1,fill=1,dim=3,bb=zoom3d,
        ps=savedir+prefix+"divu.png",cmm="Mixed Velocity Div");
}
//
//  Error report
// ____________________________________
if (ERROR) {
real errppL2 = int2d(Th)(abs(pp-pe)^2);
real errppH1 = errppL2 + int2d(Th)((dx(pp)-pedx)^2 + (dy(pp)-pedy)^2);
real errupL2 = int2d(Th)(abs(up1-ue1)^2 + abs(up2-ue2)^2);
real errpL2  = int2d(Th)(abs(p-pe)^2);
real erruL2  = int2d(Th)(abs(u1int-ue1)^2 + abs(u2int-ue2)^2);
real erruHdiv = erruL2 + int2d(Th)(abs(dx(u1)-ue1dx + dy(u2)-ue2dy)^2);
cout << "============================" << endl;
cout << "   L2 error - primal          " << endl;
cout << " ||p - ph||_0 = " << sqrt(errppL2)  << endl;
cout << " ||p - ph||_1 = " << sqrt(errppH1)  << endl;
cout << " ||u - uh||_0 = " << sqrt(errupL2)  << endl;
cout << "   L2 error - mixed           " << endl;
cout << " ||p - ph||_0 = " << sqrt(errpL2)   << endl;
cout << " ||u - uh||_0 = " << sqrt(erruL2)   << endl;
cout << " ||u - uh||_div = " << sqrt(erruHdiv)   << endl;
cout << "============================" << endl;
}
```

References

[1] I. Babuška. Error-bounds for finite element method. *Numerische Mathematik*, 16(4):322–333, 1971.

[2] L. Bergamaschi, S. Mantica, and G. Manzini. A mixed finite element-finite volume formulation of the black-oil model. *SIAM Journal on Scientific Computing*, 20(3):970–997, 1998.

[3] D. Boffi, F. Brezzi, and M. Fortin. *Mixed finite element methods and applications*, volume 44 of *Springer Series in Computational Mathematics*. Springer, Heidelberg, 2013.

[4] D. Braess. An a posteriori error estimate and a comparison theorem for the nonconforming P_1 element. *Calcolo*, 46(2):149–155, 2009.

[5] J. Brandts, S. Korotov, and M. Křížek. Simplicial finite elements in higher dimensions. *Appl. Math.*, 52(3):251–265, 2007.

[6] F. Brezzi. On the existence, uniqueness and approximation of saddle-point problems arising from Lagrangian multipliers. *Rev. Française Automat. Informat. Recherche Opérationnelle Sér. Rouge*, 8(R-2):129–151, 1974.

[7] F. Brezzi, J. Douglas, Jr., R. Durán, and M. Fortin. Mixed finite elements for second order elliptic problems in three variables. *Numer. Math.*, 51(2):237–250, 1987.

[8] F. Brezzi, J. Douglas, Jr., M. Fortin, and L. D. Marini. Efficient rectangular mixed finite elements in two and three space variables. *RAIRO Modél. Math. Anal. Numér.*, 21(4):581–604, 1987.

[9] F. Brezzi, J. Douglas, Jr., and L. D. Marini. Recent results on mixed finite element methods for second order elliptic problems. pages 25–43, 1986.

[10] F. Brezzi and M. Fortin. *Mixed and hybrid finite element methods*, volume 15 of *Springer Series in Computational Mathematics*. Springer-Verlag, New York, 1991.

[11] C. Carstensen, D. Peterseim, and M. Schedensack. Comparison results of finite element methods for the Poisson model problem. *SIAM J. Numer. Anal.*, 50(6):2803–2823, 2012.

[12] R. Courant. Variational methods for the solution of problems of equilibrium and vibrations. *Bull. Amer. Math. Soc.*, 49:1–23, 1943.

[13] M. Crouzeix and P.-A. Raviart. Conforming and nonconforming finite element methods for solving the stationary Stokes equations. I. *Rev. Française Automat. Informat. Recherche Opérationnelle Sér. Rouge*, 7(R-3):33–75, 1973.

[14] C. D'Angelo and A. Quarteroni. On the coupling of 1d and 3d diffusion-reaction equations. application to tissue perfusion problems. *Mathematical Models and Methods in Applied Sciences*, 18(8):1481–1504, 2008.

[15] F. Hecht. New development in freefem++. *J. Numer. Math.*, 20(3-4):251–265, 2012.

[16] A.F.D. Loula, F.A. Rochinha, and M.A. Murad. Higher-order gradient post-processings for second-order elliptic problems. *Computer Methods in Applied Mechanics and Engineering*, 128(3-4):361–381, 1995.

[17] L. D. Marini. An inexpensive method for the evaluation of the solution of the lowest order Raviart-Thomas mixed method. *SIAM J. Numer. Anal.*, 22(3):493–496, 1985.

[18] A. Masud and T.J.R. Hughes. A stabilized mixed finite element method for darcy flow. *Computer Methods in Applied Mechanics and Engineering*, 191(39–40):4341 – 4370, 2002.

[19] J.-C. Nédélec. Mixed finite elements in $\mathbf{R}^3$. *Numerische Mathematik*, 35(3):315–341, 1980.

[20] W. Prager and J. L. Synge. Approximations in elasticity based on the concept of function space. *Quart. Appl. Math.*, 5:241–269, 1947.

[21] A. Quarteroni. *Numerical models for differential problems*, volume 8 of *MS&A. Modeling, Simulation and Applications*. Springer, Milan, second edition, 2014. Translated from the fifth (2012) Italian edition by Silvia Quarteroni.

[22] A. Quarteroni and A. Valli. *Numerical approximation of partial differential equations*, volume 23 of *Springer Series in Computational Mathematics*. Springer-Verlag, Berlin, 1994.

[23] P.-A. Raviart and J. M. Thomas. Primal hybrid finite element methods for 2nd order elliptic equations. *Mathematics of Computation*, 31(138):391–413, 1977.

[24] F. Williamson, Jr. Richard Courant and the finite element method: a further look. *Historia Math.*, 7(4):369–378, 1980.